

1 **Aerosol and trace-gas measurements in the Darwin area during**  
2 **the wet season**

3

4 **G. Allen<sup>1</sup>, G. Vaughan<sup>1</sup>, K. N. Bower<sup>1</sup>, P. I. Williams<sup>1</sup>, J. Crosier<sup>1</sup>, M. Flynn<sup>1</sup>,**  
5 **P. Connolly<sup>1</sup>, J. F. Hamilton<sup>2</sup>, J. D. Lee<sup>2</sup>, J. E. Saxton<sup>2</sup>, N. M. Watson<sup>2</sup>, M.**  
6 **Gallagher<sup>1</sup>, H. Coe<sup>1</sup>, J. Allan<sup>1</sup>, T. W. Choularton<sup>1</sup>, A. C. Lewis<sup>2</sup>**

7

8 [1] {Centre for Atmospheric Science, Sackville St Building, Sackville St, University of Manchester,  
9 Manchester, M60 1QD}

10 [2] Department of Chemistry, University of York, Heslington, York, YO10 5DD, UK.

11 Correspondence to: G. Allen ([grant.allen@manchester.ac.uk](mailto:grant.allen@manchester.ac.uk))

1 **Abstract**

2 The composition of the planetary boundary layer in regions of deep tropical convection  
3 has a profound impact on the Tropical Tropopause Layer (TTL). The Aerosol and  
4 Chemical Transport in tropical conVEction (ACTIVE) aircraft campaign was conducted  
5 from November 2005 to February 2006 from Darwin, Australia, to characterise the  
6 influence of both monsoonal and localised land-based deep convection on the  
7 composition of the TTL. This paper summarises the composition of the potential inflow  
8 to such convection in terms of aerosol particle size and composition, carbon monoxide  
9 and ozone, as measured in the lowest 4 km of the atmosphere by the NERC Dornier-228  
10 aircraft during 28 flights in different meteorological regimes over the course of ACTIVE.  
11 Six contrasting periods are identified in the boundary layer background as a result of the  
12 prevailing meteorology and sources of pollution. The campaign began with a relatively  
13 polluted and variable biomass burning season in November, followed by a transition to  
14 the monsoon season through December with much less burning. A clean maritime flow  
15 dominated the wet-active, and dry-inactive, monsoon period in January; followed by a  
16 monsoon break period in February, with a return to continental flow and a more pre-  
17 monsoon background state. Deep convective systems, capable of transporting boundary  
18 layer air to the TTL were observed daily outside of the monsoon periods. The chemical  
19 composition of sub-micron aerosols in the pre-monsoon periods was dominated by a mix  
20 of fresh and aged organic material with significant black carbon, well-correlated with  
21 carbon monoxide indicating a common burning source, whilst marine aerosol during the  
22 monsoon changed markedly between the wet and dry phases. High concentrations of  
23 coarse-mode aerosols were also observed in the monsoon - the clean, marine air masses

1 and high surface winds imply that sea salt may be the dominant aerosol type under these  
2 conditions. The climatology presented here will provide a valuable dataset for model  
3 simulation of chemical and aerosol transport by deep convection in the Darwin region.

## 1 **1 Introduction**

2

3 Tropical convection is a crucial issue for climate science for many reasons: Tropical  
4 cloud composition (e.g. ice water, liquid water, black carbon) and cloud-top-height have  
5 profound implications for the Earth's radiative budget; and fast transport (a few hours) of  
6 surface boundary layer trace gases and particles to the upper troposphere affect its  
7 composition and chemistry [Dessler, 2002]. The *Tropical Tropopause Layer* (TTL) is the  
8 subject of much ongoing study to reduce uncertainty in climate change predictions and  
9 the nature of stratosphere-troposphere exchange [Stohl *et al.*, 2003] and consequent  
10 impacts on stratospheric ozone [Esler *et al.*, 2001]. Furthermore, aerosol particles lifted  
11 from the surface have indirect effects influencing precipitation and radiation fluxes  
12 [Lohmann and Feichter, 2005; McFiggans *et al.*, 2006]. For example, the convective  
13 uplift of black carbon aerosol generated by frequent biomass burning in the tropics can  
14 perturb the radiative equilibrium of the atmosphere; with both the sign and magnitude of  
15 the resultant net forcing noted to be highly uncertain and highly dependent on the overall  
16 particle composition and position in the atmosphere [IPCC, 2001]. Therefore, a better  
17 knowledge of tropical boundary layer composition is implicit in a better understanding of  
18 tropical convection and better characterisation of the TTL environment.

19 The UK Natural Environment Research Council (NERC)-funded ACTIVE  
20 campaign described by Vaughan *et al.*, [2007], was conceived as a comprehensive  
21 research program of field measurements and modelling work to address these key  
22 scientific questions. This campaign took place during the 2005/2006 wet season  
23 (November – February) in Darwin, Australia (12.47°S, 130.85°E), and employed two

1 aircraft: the Dornier 228-101 operated by the NERC Airborne Research and Survey  
2 Facility, and the Grob G520T Egrett aircraft operated by Airborne Research Australia.  
3 Instrumentation on the Dornier measured the aerosol and chemical background of the  
4 boundary layer and lower free troposphere between 100 and 4000 m (see next section),  
5 whilst the Egrett measured cirrus cloud microphysics and outflow from deep convection  
6 up to an operational ceiling of 15 km. Furthermore, a total of thirty-five ozonesondes  
7 were launched throughout the campaign from Darwin Airport to provide simultaneous  
8 profiles of horizontal winds, pressure, temperature, relative humidity and ozone  
9 concentration.

10 ACTIVE was one component of a comprehensive field experiment conducted  
11 during 2005/2006 to study TTL composition and clouds in the Darwin region, the other  
12 two being the SCOUT-O3 campaign between 15 November 2005 and 8 December 2005  
13 also described by *Vaughan et al.*, [2007], and the Tropical Warm Pool International  
14 Cloud Experiment (TWP-ICE) conducted between 21 January 2006 and 14 February  
15 2006. Further aircraft measurements in the TTL, and meteorological measurements in the  
16 boundary layer, were conducted by these projects, while radiosondes were launched  
17 every six hours as part of TWP-ICE from a network of locations around Darwin during  
18 TWP-ICE. Together, these synergistic campaigns generated an unprecedented dataset  
19 from which to study tropical deep convection.

20 The Darwin region offers a unique location from which to conduct studies of  
21 tropical convection, due to its proximity to the tropical warm pool around Indonesia and  
22 to the Tiwi Islands situated 150 km to the north. So-called Hector thunderstorms occur  
23 almost daily over the Tiwis during the pre-monsoon and monsoon-break periods between

1 November and February as a result of the strong convergence of warm, moist sea and  
2 land breezes [Crook, 2000]. In addition, the annual monsoon flow initiates large-scale  
3 uplift in the area [Manton and McBride, 1992]. In order to understand the impact on the  
4 TTL of these convective influences it is necessary to first understand the composition of  
5 the boundary layer and hence the inflow to local convective storms in order to relate  
6 observations of the high-altitude outflow with those made in the inflow region. This  
7 paper derives representative summaries of gas phase and aerosol size and composition  
8 data measured by the NERC Dornier aircraft for various meteorological regimes  
9 encountered during ACTIVE.

10         The main sources of aerosol expected around the Darwin area are from biomass  
11 burning, the local maritime environment and possible dry soil disturbance - potentially  
12 lofting mineral dust. Biomass burning in the northern Australian savanna occurs very  
13 frequently throughout the dry season (June to November) with average annual fuel  
14 loadings of up to  $9.2 \text{ t ha}^{-1}$  as estimated by Russell-Smith *et al.*, [2003], for the nearby  
15 Arnhem Land region during 1999. Fire maps derived using the method described Giglio  
16 *et al.*, [2003] and Davies *et al.*, [2004], from the Moderate Resolution Imaging  
17 Spectroradiometer (MODIS) instrument on NASA's TERRA satellite, are shown in  
18 Figure 1, which show the prevalence of biomass fires across the Northern Territory in  
19 November 2005 (Fig. 1a); and in contrast, an absence of such fires in the region by  
20 December (Fig. 1b) and a continued absence into late January (Fig 1c). Fires in the  
21 Queensland region (over 1500 km to the east) are evident at all times throughout the  
22 campaign, with greater intensity during November/December than in January/February.

1 Burning emissions in the Northern Territory were extensively studied by the  
2 Biomass Burning and Lightning Experiment (BIBLE) campaign described by *Kondo et*  
3 *al.*, [2003], which concentrated predominantly on gas phase emissions and the wider  
4 Asian and Indonesian environment, with some observations of aerosols and black carbon  
5 [*Liley et al.*, 2002]. The bulk of such burning early in the dry season is initiated by land  
6 managers and is relatively low in intensity to remove denser undergrowth that has built  
7 up over the preceding wet season. Towards the end of the dry season, fires become more  
8 intense as drier fuel sources are consumed. This is particularly the case in Arnhem Land  
9 to the east of Darwin, where grassy fuel dries out later in the year compared with the  
10 western regions, and is thus prone to fires being started due to lightning or accident. On  
11 any given day, the number and location of fires can vary greatly with background smoke  
12 levels between June and September reported to change markedly [*Carr et al.*, 2005], with  
13 a tendency toward increasing smoke accumulation and larger particle sizes throughout the  
14 period. Hence we expect such burning to influence the local boundary layer for the first  
15 weeks of the ACTIVE campaign, when prevailing surface winds were easterly (see  
16 Section 4).

17 In contrast to the pre-monsoon, maritime air is expected to dominate during active  
18 monsoon episodes, albeit with the potential for mixing of transported continental  
19 airmasses. To our knowledge, no previous studies of the aerosol background in Northern  
20 Australia during the wet season have taken place, a need highlighted by *Heintzenberg et*  
21 *al.*, [2000].

22 The boundary layer CO burden near Darwin is expected to show a general  
23 relationship to the aerosol burden, reflecting the nature of common pyrogenic sources.

1 However, episodic influences of long-range transport of pollutants to northern Australia  
2 from sources such as South America and South Africa in austral spring have been  
3 reported for CO as retrieved from satellite observations [*Gloude-mans et al.*, 2006]. Hence  
4 we see that the Darwin boundary layer environment is influenced not only by local  
5 sources but also by the governing meteorology and potentially more distant sources of  
6 pollution. This paper aims to illustrate this contrast throughout typical meteorological  
7 regimes encountered between November and February in the region.



## 1 **2 The Dornier-228: Mission and Instrumentation**

### 2 **2.1 Aerosol and gas inlet**

3 The Dornier-228 is a light twin-engine aircraft with an interior cabin modified to harbour  
4 a scientific payload. Ambient air was sampled through a purpose-built stainless steel,  
5 forward-facing, passive, isokinetic inlet positioned over the centre of the cockpit (see Fig.  
6 2). The inlet was manufactured by Deutsche Zentrum für Luft und Raumfahrt (DLR) and  
7 based on the aerosol inlet on the DLR Falcon aircraft. Transmission for this inlet is  
8 calculated to be 95% at 0.9  $\mu\text{m}$ , 75% at 1.6  $\mu\text{m}$  and 50% at  $\sim 2.5$   $\mu\text{m}$  particle diameter. For  
9 further technical information relating to this inlet see *Fiebig*, [2000], and *Petzold et al.*,  
10 [2001]. From the main aerosol manifold, two isokinetic sub-samples were taken: one  
11 branch fed the aerosol spectrometers and a particle soot absorption photometer (detailed  
12 in Section 2.3) on the port side of the aircraft, with the other feeding an aerosol mass  
13 spectrometer, a condensation particle counter and deposition filters on the starboard side.  
14 Each branch was further split isokinetically to feed the individual instruments. The gas  
15 phase instruments were fed from a rearward-facing inlet on the main manifold (see Fig.  
16 2), whilst the exhaust from all instruments vented to the aft of the cabin. Transmission  
17 and diffusive losses after the inlet were calculated using aerodynamic theory outlined by  
18 *Baron and Willeke*, [1993], and were found to be negligible across the size range of  
19 particles discussed in this work up to the 50% transmission cut-off diameter of the main  
20 inlet (2.5  $\mu\text{m}$ ). Hence, transmission losses were dominated by the main inlet for super-  
21 micron particles.

## 1 **2.2 Thermodynamic instrumentation.**

2 Temperature, pressure, relative humidity and wind vectors, as well as GPS position and  
3 aircraft orientation, were sampled at 20 Hz and recorded at 1 Hz by a Aircraft Integrated  
4 Meteorological Measuring System (AIMMS) 20 Hz probe manufactured by *Aventech*  
5 *Research Inc.* and described further by *Beswick et al.*, [2007]. The probe was positioned  
6 on a starboard wing-mounted pod. Typical air speed and aircraft pitch angle on science  
7 runs were  $75 \text{ ms}^{-1}$  and  $+4.5^\circ$  respectively.

## 8 **2.3. Aerosol Instrumentation**

9 *Number and size:* Aerosol particle number size distributions from 55 nm to 32  $\mu\text{m}$   
10 diameter were measured using a range of optical probes (see Table 1). Herein, the terms  
11 *fine mode* and *coarse mode* aerosol refer to the sub-micron and super-micron aerosol  
12 population fraction respectively. Optical scattering instruments included:

13 (i) a Droplet Measurement Technologies (DMT, Boulder, CO, USA) ultra high sensitivity  
14 aerosol spectrometer (UHSAS), measuring dry fine mode aerosol size spectra at 1 Hz  
15 (averaged to 1/6 Hz) with a fine size resolution (7.5 nm bins) in the range 55 nm to 800  
16 nm.

17 (ii) A prototype DMT aerosol spectrometer probe (ASP), measuring dry aerosol with a  
18 resolution between 0.1 and 0.2  $\mu\text{m}$  in the range 0.21 to 4.5  $\mu\text{m}$ .

19 (iii) A Grimm Aerosol Technik (GmbH) 1.108 optical particle counter (Ainring,  
20 Germany), measuring dry size ranges with a resolution between 0.03 and 0.5  $\mu\text{m}$  in the  
21 range 0.3 to 25  $\mu\text{m}$ .

1 (iv) for the coarse aerosol component, a wing-mounted forward scattering spectrometer  
2 probe (FSSP-100), described further by *Baumgardner et al.*, [1985], measuring ambient  
3 particle number size distributions with resolution 0.8  $\mu\text{m}$  from 0.5 to 32  $\mu\text{m}$ .

4 In addition, a TSI-3010D (TSI Inc., Shoreview, MN, USA) condensation particle counter  
5 (CPC) measured the total particle number concentration greater than  $\sim 10$  nm. However,  
6 absolute number concentrations for sizes greater than 2  $\mu\text{m}$  measured by the ASP and  
7 Grimm instruments are not considered here due to inlet transmission limitations (50%  
8 transmission at 2.5  $\mu\text{m}$ )

9 *Black carbon:* A Radiance Research Inc particle soot absorption photometer (PSAP)  
10 measured black carbon content. For this study, the soot absorption cross-section  
11 ( $\sigma_{ae} = 8.2 \text{ m}^2 \text{ g}^{-1}$ ) used by *Liley et al.*, [2002], for the geographically similar BIBLE  
12 campaign is assumed. To account for high measurement noise, 0.2 Hz PSAP data were  
13 smoothed over a five-minute period. In stable operating conditions the PSAP sensitivity  
14 to changes in filter absorption gives a precision of  $10^{-6} \text{ m}^{-1}$ , or roughly  $0.02 \mu\text{g m}^{-3}$  of soot  
15 for five-minute integration.

16 *Composition:* A Quadrupole Aerodyne Aerosol Mass Spectrometer (Q-AMS) system  
17 [*Jayne et al.*, 2000], which sampled air through the main manifold, was used to determine  
18 the mass loading of the non-refractory, non sea-salt chemical component of sub-micron  
19 aerosol with a high time resolution (30 seconds). This instrument employs thermal  
20 desorption, 70 eV electron ionisation, and a quadrupole mass spectrometer. Data were  
21 processed and quality assured using the procedures described by *Jimenez et al.*, [2003],  
22 and *Allan et al.*, [2003, 2004a], and employed in conjunction with the pressure-dependent  
23 calibrations and corrections described by *Crosier et al.*, [2006], needed for aircraft

1 operation. Mass concentrations are reported from the Q-AMS (see Section 5) for the total  
2 nitrate, organic, sulphate and ammonium component masses in the aerosol. Component  
3 mass size distributions could not be derived here with sufficient confidence (reasonable  
4 signal to noise) due to the relatively clean environment sampled throughout the majority  
5 of ACTIVE flights.

#### 6 **2.4. Gas phase instrumentation**

7 Gas phase instruments onboard the Dornier are summarised in Table 2 and consisted of:

8 *Carbon monoxide:* Measurement of CO was performed in-flight using a fast response  
9 fluorescence instrument; the AL5002 fast carbon monoxide (CO) monitor (Aero-Laser  
10 GmbH, Garmisch-Partenkirchen, Germany), fitted with a Nafion dryer to remove water  
11 vapour. With an integration time of ten seconds, the detection limit was better than 2.0  
12 ppbv. The linearity range of the instrument was 0 – 100 ppmv; well beyond the typical  
13 concentrations encountered during ACTIVE. Calibration of the instrument was  
14 performed in-flight at various flight levels to allow for the potential effect of ambient  
15 pressure changes, using a secondary gas standard containing 73 ppbv  $\pm$  5 % CO in  
16 synthetic air. An additional standard (200 ppbv) was used throughout the campaign to  
17 validate the in-flight standard. Data were recorded at one-second intervals.

18 *Ozone:* Ozone was measured in-flight using a UV absorption detector (2B  
19 Technologies). Calibration was carried out prior to deployment using gas phase titration  
20 of NO. Data were collected at ten second intervals with an overall uncertainty of 5 % ( $\pm$   
21 2 ppbv). Concentration resolution is approximately 1 ppbv.

22 *Volatile Organic Compounds (VOCs):* Additional measurements of a range of VOCs  
23 were also obtained onboard the Dornier using adsorbent tube samplers and post-flight

1 thermal desorption coupled to comprehensive two-dimensional gas chromatography with  
2 time-of-flight mass spectrometry (see *Hamilton et al.*, [2007], and *Saxton et al.*, [2007],  
3 for further details). Calibration was achieved using a 74 component gas standard at 0.1 –  
4 2 ppbv levels (Apel Reimer) and uncertainties on single measurements of all VOCs  
5 derived by this method are typically around 20 % of the determined concentration..  
6 Species measured include: isoprene,  $\alpha$ -pinene, ethyl benzene, m+p xylene, o-xylene,  
7 nonane, isopropyl benzene, 3-ethyl toluene, 1, 3, 5-trimethyl benzene, 1, 2, 4- trimethyl  
8 benzene, and 1, 2, 3- trimethyl propyl benzene. Isoprene and  $\alpha$ -pinene are not discussed  
9 further here due to their very low atmospheric lifetimes (of the order 1 hour) and high  
10 spatial variability (e.g. land/sea contrast) making any overall analysis of their  
11 concentration meaningless.

### 12 **2.3 Flight operations**

13 A total of eleven Dornier science flights and one test flight were carried out in the first  
14 phase of the campaign between 13 November and 5 December 2005, of which eight were  
15 circumnavigations of the Tiwi Islands to the north of Darwin during the development of  
16 Hector-type convection, and three were survey flights of the wider Darwin region (See  
17 Table 3 for a summary). A further sixteen flights were conducted in the second phase  
18 between 19 January and 14 February 2006, of which three were survey flights of the  
19 wider region, four studied the inflow to monsoon convection and a further four measured  
20 inflow to Hector systems.

21 Other flights in the second phase included two survey flights to study a monsoon  
22 trough inland between Darwin and Alice Springs and a further two flights to sample  
23 potentially contrasting airmasses toward Indonesia. These four flights are not considered

1 further here as they are not relevant to the climatological background of convective  
2 inflow near Darwin. An additional flight was performed to compare simultaneous  
3 measurements alongside the Egrett aircraft (see next section) for the purposes of  
4 instrument intercomparison.

### 1 **3. Data Quality**

#### 2 **3.1. Meteorological data quality**

3 Meteorological measurements made by the AIMMS-20 probe were compared with  
4 radiosonde profiles launched from Darwin Airport and additionally with the six-hourly  
5 TWP-ICE radiosonde network in January and February. Comparisons of the AIMMS  
6 temperature measurements with closely coincident radiosondes gave random differences  
7 of  $\pm 1^\circ\text{C}$ . Due to horizontal variability in temperature these differences are not  
8 considered significant and no corrections were applied to the data. The instrument  
9 manufacturers claim an accuracy of  $0.3^\circ\text{C}$  for AIMMS temperature.

10 Relative humidity (RH), static pressure and wind data recorded by the AIMMS  
11 probe were compared with the sonde dataset and with Rotronic HygroClip SC05  
12 temperature and humidity sensors in the AMS sample line. A direct quantitative  
13 comparison of AIMMS RH with sondes is limited by the very high natural horizontal  
14 variability; however, no systematic differences were noted in November and December  
15 and the AIMMS and Rotronic sensors agreed to within 10% (after correcting the latter for  
16 the temperature and pressure difference between the atmosphere and inlet line). In the  
17 second phase of the campaign, the AIMMS probe was noted to have developed a  
18 technical problem due to contamination, with frequently recorded unrealistic RH in  
19 excess of 120% and consistent differences of up to 60% between AIMMS and Rotronic  
20 sensors. Therefore, RH measurements (corrected for ambient pressure and temperature)  
21 recorded by the Rotronic sensor are used for all Dornier flights in the second phase of  
22 ACTIVE.

1           General agreement in horizontal wind direction and wind speed was found  
2 between radiosondes and AIMMS, and AIMMS pressure was noted to be highly  
3 consistent (to within 1 mb) with sonde profiles of pressure at equivalent altitudes.

#### 4 **3.2 Aerosol Data Quality**

5 The multiplicity of aerosol spectrometer instruments with overlapping size ranges in  
6 ACTIVE allows good characterisation of each instrument and better confidence in the  
7 accuracy of quantitative data. Median values of total aerosol number concentration for the  
8 Grimm, ASP and UHSAS, in their common size range of 0.3 to 0.8  $\mu\text{m}$ , were calculated  
9 for each Dornier flight and compared.

10           The average ratio of medians from each flight between the Grimm and ASP  
11 spectrometers was  $1.71 \pm 0.26$  in the first phase of the campaign and  $1.58 \pm 0.20$  in the  
12 second phase; therefore we conclude that these two instruments were reasonably  
13 consistent with each other throughout the whole campaign, in that neither instrument  
14 developed a significant drift in sensitivity. However, the UHSAS developed a technical  
15 fault after the end of the first phase of ACTIVE and its data are considered unreliable for  
16 the later period. The Grimm and ASP worked correctly throughout the campaign, so due  
17 to its greater spectral size resolution, the fine mode aerosol number concentrations  
18 reported in this work are taken from the ASP instrument. Differences between the  
19 instruments in the first phase serve here as an indication of the inherent uncertainties in  
20 using optical probes; variations in particle shape and (complex) refractive index can  
21 result in ambiguities in the scattering properties of the aerosol under investigation [*Liu*  
22 *and Daum, 2000*].



1 For the AMS, a collection efficiency of 0.5 was used, typical of the value obtained  
2 through comparisons with other instruments in the field [*Allan et al.*, 2004b; *Takegawa et*  
3 *al.*, 2005]. This was validated through a comparison between the integrated UHSAS total  
4 particulate volume and the summed AMS and PSAP particulate volume measurements,  
5 assuming a density of  $1.77 \text{ g cm}^{-3}$  for inorganic aerosol and  $1.2 \text{ g cm}^{-3}$  for organics, as  
6 derived by *Cross et al.*, [2007]. Average ratios of UHSAS integrated volume to summed  
7 AMS and PSAP volumes were in the range 0.4 to 0.7.

### 8 **3.3 Gas Phase data quality**

9 Carbon monoxide and ozone measurements onboard the Dornier were compared with  
10 instrumentation on the Egrett aircraft during purpose-flown intercomparison flights where  
11 both flew in formation. One such flight was performed in each measurement phase.  
12 Carbon monoxide differed by 10 ppbv at most between the two aircraft's instruments so  
13 we take 10 ppbv as the uncertainty on CO data and note that the inter-seasonal variability  
14 measured during ACTIVE greatly exceeds this.

15 A comparison for ozone in the first phase was not possible due to a failure of the  
16 Egrett ozone instrument. A flight intercomparison in the second phase showed that the  
17 Dornier ozone instrument measured more than the Egrett's by  $\sim 7$  ppbv. However,  
18 problems were noted with the Egrett instrument due to systematic differences in  
19 measured concentration between ascent and descent. Dornier ozone profiles were also  
20 compared with ozonesondes launched from Darwin Airport (where available). Although  
21 differences of up to 10 ppbv were observed on flights where measured spatial variability  
22 in ozone was high, with the Dornier tending to read less than the sondes on average,  
23 much of this is expected to be due to naturally high horizontal variability. On flights

1 where little spatial variability was observed in the Dornier data, and the PBL ozonesonde  
2 profile varied smoothly with altitude, differences were much smaller ( $< 2$  ppbv).

3

#### 4 **4. Prevailing Meteorology**

5 Six contrasting periods are identified here for the purposes of deriving representative  
6 climatologies on the basis of contrasting meteorology and biomass burning influences.

7 These periods and the science flights conducted in each period are summarised in Table  
8 4. Data from all flights within each period are used to derive the summaries presented in  
9 Section 5. The contrasting meteorology of each period is discussed in the remainder of  
10 this section.

11 **Biomass Burning:** During the first phase of the ACTIVE campaign, typical pre-monsoon  
12 conditions prevailed at Darwin. For most of this period the lower-level winds were  
13 dominated by easterly flow at 700 mb (the convective steering level) with wind speeds  
14 between 12 to 20  $\text{ms}^{-1}$ . At the surface, local sea-breeze circulations generated a range of  
15 convective storms, from isolated island thunderstorms to squall line complexes  $\sim 100$  km  
16 in scale. Such deep convective storm systems regularly achieved cloud top heights in  
17 excess of 18 km [Vaughan *et al.*, 2007] suggesting significant fast transport of boundary  
18 layer air to the TTL during this period. Back-trajectories of air sampled by the Dornier in  
19 the Darwin area generally tracked over Queensland and the Northern Territories over the  
20 previous five days (see Fig. 3). Large-scale land clearance burning over Arnhem Land to  
21 the east of Darwin is evident from MODIS fire maps during this period (see Fig. 1) with  
22 resulting plumes mixing into the easterly surface flow arriving at Darwin throughout this

1 period. On occasion, fresh plumes from localised active burning on the Tiwi Islands were  
2 also sampled by the Dornier.

3 **Mini-Monsoon:** An exception to this general pattern occurred between 20-22 November,  
4 during which a ‘mini-monsoon’ was experienced, so named because of a deep westerly  
5 flow from 700 mb to 200 mb coincident with widespread oceanic convection. This period  
6 was not a true monsoon in the meteorological sense, but the resultant oceanic convection  
7 and deep maritime flow greatly resembled monsoon conditions. This reversal in the  
8 prevailing winds was associated with an unusually strong northward undulation of the  
9 sub-tropical jet stream and a significant westerly momentum injection to the free  
10 troposphere associated with a breaking Rossby wave. Back trajectories initiated at 900  
11 mb and 700 mb during this time show easterly and westerly origins respectively,  
12 suggesting that clean maritime air at low levels would have been overlaid with relatively  
13 polluted air arriving from the burning regions to the east. Deep convection initiated by  
14 sea-breeze circulations was absent during these few days due to the strong wind shear  
15 associated with the passage of the Rossby wave, with the observed maritime convection  
16 reaching cloud top heights much less than 10 km.

17 **Pre-Monsoon:** Following a return to a prevailing easterly flow after the passage of the  
18 Rossby wave, back trajectories show a return to inland origins to the east and south of  
19 Darwin. However, MODIS fire maps (Fig. 1) show that the number of biomass burning  
20 sites during this period were greatly reduced. Therefore, although the general  
21 meteorology was broadly similar to the biomass burning period discussed earlier, we can  
22 expect airmasses sampled during this period to be much less influenced by local biomass  
23 burning sources. Similar sea-breeze circulations and isolated deep convective systems

1 were observed daily during this period with the potential for significant fast transport to  
2 the TTL.

3 **Active Monsoon:** Prior to the start of flight operations in the second phase of ACTIVE, a  
4 monsoon trough formed to the south of Darwin with a north-westerly monsoon flow from  
5 the surface to 300 mb developing by 14 January 2006. Back trajectories from Darwin  
6 during this period show a long-range westerly maritime origin for at least 5 days prior to  
7 sampling. Large scale maritime convection was prevalent during this time with cloud top  
8 heights reaching up to the tropopause. This ‘active monsoon’ period persisted until 22  
9 January 2006, when a monsoon low formed just to the north of Darwin and moved  
10 southward to the central Northern Territory.

11 **Inactive Monsoon:** The inland monsoon low dominated the meteorology in the Darwin  
12 area until 3 February 2006, bringing a stable westerly airstream in the lower troposphere  
13 across the Darwin area which suppressed deep convection, with storms generally  
14 reaching no higher than 10 km. We refer to this period as the *inactive monsoon*.

15 **Monsoon Break:** After 3 February, the monsoon low disappeared, and easterly flow  
16 gradually developed – initially at 700 mb but eventually leading to a deep easterly airflow  
17 as in the pre-monsoon period. Isolated deep convection became prevalent, initially as  
18 Hector storms over the Tiwi Islands, then eventually extending to the mainland giving  
19 similar conditions to the pre-monsoon. Convection also became more organised: single-  
20 cell Hector storms were observed on 6 February, intensifying to become multi-cellular  
21 from 9 February until the end of the campaign.

## 1 **5. Results**

### 2 **5.1 Carbon Monoxide and Ozone**

3 Vertical profiles of median carbon monoxide (CO) and ozone concentration for each time  
4 period are plotted in Figure 4 together with upper and lower quartiles and 10<sup>th</sup> and 90<sup>th</sup>  
5 percentile whiskers. Data were averaged across those flights within each period in Table  
6 4 within three vertical layers between 0 - 3 km with 1 km resolution and an additional  
7 box for altitudes greater than 3 km (note that the maximum altitude flown by the Dornier  
8 in the campaign was 4.1 km). To ensure that data used here are not contaminated by  
9 sources associated with airstrips (e.g. other aircraft, generators, etc.), all data below 100  
10 m during take-off and landing have been discarded. Furthermore, very short-lived high  
11 concentrations (data spikes) have been removed; these probably occurred when engine  
12 exhaust was sampled due to turbulent flow in steep ascending turns. More complete  
13 statistics averaged over all altitudes for each period are summarised in Table 5.

14 Carbon monoxide is a useful, relatively long-lived (~2 months in the troposphere)  
15 tracer of many land-based pollution sources [*Staudt et al.*, 2000]. In the southern  
16 hemisphere the lack of strong anthropogenic fossil fuel sources makes CO a predominant  
17 marker of both fresh and aged biomass burning plumes and is typically well-correlated  
18 with aerosol number concentration [e.g. *Edwards et al.*, 2006]. In conjunction with ozone  
19 concentration and aerosol composition such as that afforded here by the AMS, CO can  
20 also be used to differentiate source-type and age of polluted airmasses. Carbon monoxide  
21 is discussed here in this context as a tracer of airmass origin and an indicator of  
22 background pollution levels.

1           Figure 4 shows a clear evolution in background CO. In the biomass burning  
2 season, we see not only the highest levels of CO (~102 ppbv), but also the largest  
3 variability with a distribution extending to values in excess of 150 ppbv. The inter-  
4 quartile range is small relative to the difference between the 75<sup>th</sup> and 90<sup>th</sup> percentiles,  
5 reflecting a small number of very high CO events, which are associated with short flight  
6 legs targeted at sampling visually polluted layers (smoke) in fresh fire plumes. In the  
7 mini-monsoon period, there is a little less CO (~90 ppbv) in the background atmosphere  
8 and variability is reduced. This is consistent with the introduction of cleaner maritime air  
9 in the westerly flow during this period, coupled with a reduction in the intensity of fires  
10 inland due to increased rainfall. However, the general background is still high in CO  
11 (relative to succeeding periods) and therefore better characterised in terms of burning  
12 influences. The pre-monsoon is cleaner still with an overall median concentration of 86  
13 ppbv and much less variability than the burning-dominated period. This pre-monsoon  
14 period represents similar meteorology to the polluted burning season, with the major  
15 difference being the absence of inland fires.

16           Throughout both the active and inactive monsoon periods, CO continues to fall  
17 and shows very low variability within each period as cleaner maritime air was drawn into  
18 the Darwin area from the west. In the cleanest period (51 ppbv in the inactive monsoon),  
19 ten-day back trajectories indicate advection from the remote Southern Ocean associated  
20 with circulation around the dominant inland depression throughout this period. The  
21 monsoon break shows a slight increase in CO (~58 ppbv), expected to be due to build up  
22 from local sources and longer-range transport of continental air shown by back-trajectory  
23 analysis.

1 Ozone, unlike CO, is a relatively short-lived (~1 week) species, with production  
2 and loss rates being highly dependent on the local chemical environment (e.g. NO<sub>x</sub>).  
3 Ozone was very low (around 20 ppbv for much of the campaign) in comparison to  
4 northern hemispheric background concentrations (e.g. 64 ppbv in the central US reported  
5 by *Lefohn et al.*, [2001]) and showed little change between periods. However, median  
6 ozone concentrations do exhibit the same general trend as CO, with the exception of the  
7 mini-monsoon period, which also showed greater vertical structure than the other periods.

8 Regression of CO and ozone during each period revealed positive correlations in  
9 the burning season and mini monsoon, with  $R^2 = 0.24$  and  $0.28$  respectively, and  
10 essentially no correlation thereafter, with  $R^2 = 0.07$ ,  $0.07$  and  $0.02$  in the pre-monsoon,  
11 active and inactive monsoon periods respectively. This is consistent with back trajectories  
12 over burning sites in the pre-monsoon phases and a contrasting clean maritime flow in the  
13 monsoon phases. There is a return to a positive correlation in the monsoon break ( $R^2 =$   
14  $0.18$ ) where back trajectories return to a continental origin and hence continental sources.  
15 In general, we can conclude that ozone concentrations were low and followed a similar  
16 inter-seasonal trend to CO throughout the campaign.

## 17 **5.2 Volatile organic Compounds**

18 Statistical medians, maxima and minima for the nine VOCs detailed in Section 2.4 are  
19 summarised in Table 6 for each meteorological period. By virtue of their short  
20 atmospheric lifetimes and resulting high spatial variability, VOC concentrations are more  
21 suited to a case study analysis; however, maxima and minima provided here give an  
22 indication of the general inter-seasonal trend. Concentrations of all VOCs were enhanced  
23 in the burning and pre-monsoon phases as may be expected due to their release by

1 burning vegetation. There was a general decrease in the pre-monsoon period when this  
2 burning stopped, with median concentrations for all species remaining relatively low  
3 throughout the monsoon periods and the monsoon break. Maximum concentrations for  
4 many species measured in the inactive monsoon phase exceeded those measured even  
5 during the burning season, but these represent measurements made in a pollution plume  
6 from Darwin measured on a single flight.

### 7 **5.3 Aerosol size distributions**

8 Vertical distributions of total aerosol number concentration derived in the same manner  
9 as for CO and ozone are plotted in Figure 5 from the ASP and FSSP, with total number  
10 being that integrated over the size ranges 0.3 to 2.5  $\mu\text{m}$ , and 2.5 to 32  $\mu\text{m}$  for the two  
11 instruments respectively. The size range integrated for each instrument was based on the  
12 50% transmission of the inlet ( $\sim 2.5 \mu\text{m}$ ) in the case of the ASP and the upper size range  
13 measurable by the FSSP. As spectra recorded by the ASP measure dry aerosol, and the  
14 FSSP samples aerosol at ambient humidity, the ASP spectra were transformed to ambient  
15 sizes. This was done using the model described by *Topping et al.*, [2005], and ambient  
16 humidities measured by the AIMMS-20 or Rotronic sensors of the Q-AMS as appropriate  
17 (see Section 3.1) together with aerosol compositions measured by the Q-AMS. As only  
18 total submicron component masses were available, the components were assumed to be  
19 internally mixed in the same proportions at all sizes in the accumulation mode. *Topping*  
20 *et al.*, [2005], have shown that the approach is capable of accurately predicting the  
21 growth factor of mixed component aerosol, and that for mixed inorganic-organic aerosol  
22 this growth factor is small. It is of course possible that when significant sea spray  
23 aerosols are present, the wet size of the aerosol will be significantly enhanced. This



1 would lead to an under-prediction of the ambient size of the aerosol measured by the ASP  
2 as sea salt was not measured by the AMS. Growth factors were applied using an  
3 exponential fit to the slope of the dry size spectra prior to sub-sampling each size channel  
4 into twenty and resampling the grown population into the original size grid. For the  
5 FSSP, data were cloud-cleared using a threshold value of 2 particles per ml integrated  
6 over the instrument's size range. Furthermore, due to the low sensitivity of the FSSP in  
7 such a clean environment and hence the poor counting statistics, FSSP data were  
8 averaged over a five-minute period to obtain meaningful (non-zero) median  
9 concentrations. For both the ASP and FSSP, recorded data were normalised to standard  
10 temperature and pressure (20 °C, 1001.25 mb) using simultaneously-recorded AIMMS-  
11 20 data. This pattern of diminishing aerosol number with height is similar to that seen by  
12 *Liley et al.*, [2002], in the same geographical area and is consistent with dynamics of  
13 aerosol source and deposition processes from the surface.

14 Differences in the pattern of total number between these two instruments  
15 throughout the campaign serve to illustrate changes in the fine and coarse aerosol sizes, to  
16 which the ASP and FSSP are respectively sensitive. Fine mode aerosols are important  
17 when considering scattering of ultra-violet and visible radiation and serve as efficient  
18 cloud condensation nuclei (CCN), whilst the coarse mode contains the majority of the  
19 mass and surface area of the aerosol burden, therefore playing an important role in  
20 atmospheric chemical processes.

21 The fine aerosol (ASP; Figure 5a) component varied in the same way as CO  
22 throughout the campaign (Figure 4a), with the highest and most variable concentrations  
23 measured in the burning period. The high concentrations at that time are explained by the

1 production of smoke from burning vegetation, whilst the high variability reflects the  
2 nature of day-to-day changes in inland fire activity and mixing with cleaner air. There  
3 follows a decrease in the fine aerosol concentration and associated variability at the  
4 cessation of land-clearance, with a continued decrease throughout the pre-monsoon and  
5 monsoon periods, followed by a slight recovery toward a more pre-monsoon background  
6 in the monsoon break. This difference in fine aerosol concentration between the burning  
7 phase and the inactive monsoon is in excess of an order of magnitude, with  
8 concentrations in the inactive monsoon approaching the limit of instrument sensitivity.

9         This association between CO and fine mode aerosol is also evident from their  
10 positive correlations, which are calculated to be highly significant in the biomass burning  
11 and mini-monsoon periods with  $R^2$  values of 0.46 and 0.31 respectively. Such a  
12 correlation is essentially absent in the pre-monsoon, active and inactive monsoon phases  
13 with  $R^2$  values of 0.07, 0.05 and 0.02 respectively, before a return to a significant link in  
14 the monsoon break ( $R^2 = 0.3$ ). This mirrors the trend (and significance) in correlations  
15 calculated between CO and ozone (see Section 5.1). Therefore, we can conclude that  
16 sources of fine aerosol are closely linked to sources of CO during the biomass burning,  
17 mini-monsoon and pre-monsoon periods, with the dominant source being inland biomass  
18 burning during November. The lack of any correlation between fine aerosol and CO  
19 concentration in the monsoon phases, coupled with the very small absolute number  
20 concentrations of fine aerosol in the active and inactive monsoon periods reflects both the  
21 absence of local sources and the efficient removal of these particles in maritime air via  
22 precipitation.

1           The coarse aerosol (FSSP; Figure 5b) component follows this same decreasing  
2 trend prior to the monsoon; but in contrast to the fine-mode, which is lower in the  
3 monsoon periods, we see a large increase in both median number concentration and  
4 variability in the monsoon periods compared with the pre-monsoon and the monsoon  
5 break. This change is further illustrated in median size spectra (see Figure 6a, 6b, 6c).  
6 Maxima in the accumulation and coarse modes are observed consistently near 0.3  $\mu\text{m}$  and  
7 10  $\mu\text{m}$  respectively, although the absence of reliable spectral data below 0.2  $\mu\text{m}$  obscures  
8 resolution of the fine mode maximum (see Figure 6c). A consistent peak in one size  
9 channel of the FSSP at 8.4  $\mu\text{m}$  is thought to be an instrument artefact. A further potential  
10 aerosol mode observed at 0.8  $\mu\text{m}$  is also noted in measurements by the UHSAS  
11 instrument and has been noted in previous studies by *Russell-Smith et al.*, [2000], of  
12 aerosol on the ground in the nearby town of Jabiru using a Grimm spectrometer.

13           Excellent continuity is seen in the spectra from fine to coarse particle modes  
14 measured in the pre-monsoon periods, but there is a pronounced divergence between  
15 spectra measured by the ASP and FSSP in the monsoon phases (the green and grey lines  
16 in Fig 6a, 6b and 6c). As a check of the validity of super-micron aerosol data measured  
17 by the FSSP, aerosol spectra were compared with a Cloud Aerosol Spectrometer (CAS)  
18 onboard the Egrett during its ascent and descent (0.1-3 km) flight phases within their  
19 common particle size range. Both instruments compared well, with identical trends and  
20 variability observed throughout the campaign.

21           The AMS could not measure the sea salt component of the aerosol, which would  
22 have a much larger growth factor than the sulphate/organic mix which it did measure -  
23 2.91 compared with 1.21 according to the model used here. The discrepancy between

1 FSSP and ASP during the monsoon is consistent with the aerosol having a much higher  
2 salt content than in the pre-monsoon. To test this hypothesis, dry aerosol spectra  
3 measured by the ASP were transformed with growth factors appropriate to pure sea salt  
4 aerosol. The results are shown in Figures 6d, 6e and 6f, and show a much improved  
5 spectral continuity with the measured ambient FSSP spectra. The remaining discrepancy  
6 at super-micron sizes can be explained by inlet transmission losses for the ASP, and the  
7 likely uncertainty in the measurements (see section 3.2)

8         During the monsoon periods, back trajectories remained over the ocean for at least  
9 five days prior to sampling. Any coarse-mode aerosol from long-range continental  
10 sources would be removed by deposition to the ocean over this timescale. Such pure  
11 maritime aerosol have been well studied (see review by *O' Dowd et al.*, [1997]) with two  
12 distinct types identified. These are: (1) primary sea-spray aerosol produced by  
13 mechanical disruption of the ocean surface and (2) secondary aerosol in the form of non-  
14 sea-salt sulphate and organic species formed by gas-to-particle conversion processes and  
15 subsequent cloud processing. Only the former has potential significance in the coarse  
16 mode, which is a function of wind speed; with particle size and number concentration  
17 typically following an exponential function of wind speed thus:  $\log C = aU_{10} + b$ , where  
18  $C$  is the concentration,  $U_{10}$  is the 10m height wind speed and  $a$  and  $b$  are constants which  
19 depend on particle size. Many such parameterisations have been derived from various  
20 empirical data [e.g., *Vignati et al.*, 2001, *Gong*, 2003], with a strong dependence on wind  
21 speed and humidity.

22         The spectral shape of the coarse mode fraction in Fig. 6d agrees best with that  
23 predicted by *Vignati et al.*, [2001], at wind speeds in excess of  $9 \text{ ms}^{-1}$  and high relative

1 humidities (> 85%). A full discussion of such parameterisations is beyond the scope of  
 2 this paper, but we note this agreement here to conclude that the coarse mode fraction  
 3 measured in the monsoon phases of ACTIVE should predominantly be populated by sea-  
 4 salt particles. Wind speeds measured by the AIMMS-20 in the marine boundary layer  
 5 (MBL) during monsoon flights ranged from 4 to 15 ms<sup>-1</sup> with strong variance within each  
 6 flight, but generally decreasing throughout the period. Furthermore, relative humidity  
 7 remained in excess of 85% for much of this time. In noting the strong dependence of sea-  
 8 salt particle size and production on wind speed, it is postulated that the large spectral  
 9 variability measured by the FSSP may be explained by the wide range in wind speeds  
 10 observed in the monsoon period.

#### 11 **5.4 Lognormal spectral fits**

12 In order for this aerosol size climatology to be easily used by the reader we have fitted  
 13 lognormal modes to the data according to the following relationship described further by  
 14 *Pruppacher and Klett*, [1997]:

$$15 \quad \frac{dN}{dD} = \frac{N_{tot}}{D\sqrt{2\pi} \ln \sigma_g} \exp\left(-\frac{\ln^2\left(\frac{D}{D_g}\right)}{2 \ln^2 \sigma_g}\right) \quad (\text{eq. 1})$$

16 where  $N_{tot}$  is the particle number concentration (in particles cm<sup>-3</sup>),  $D$  is the particle  
 17 diameter (μm), and  $D_g$ ,  $\sigma_g$  are the number median diameter and the geometric standard  
 18 deviation of the modal distribution, respectively. For each aerosol size spectrum in each  
 19 period, two modes were fitted to the fine component and one to the coarse component.  
 20 The fine and coarse modes were fitted independently. An interactive routine was written

1 to approximately fit the lognormal modes to the size distribution data. These approximate  
2 fits were used as an initial guess in a Gauss Newton non-linear fitting technique to yield  
3 the best fit to the data by minimising the chi-square error on successive iterations. The  
4 convergent lognormal parameters and confidences for spectra grown without chloride  
5 growth factors applied are given in Table 7. Fine mode spectra with such growth factors  
6 applied were fitted best with one mode and are given separately in Table 8.

7 For the periods without sea salt, the data are well described by the superposition  
8 of two lognormal modes; a narrow mode with high concentration in the head of the  
9 distribution and a broad mode of typically one hundred times less concentration that  
10 extended out to the tail of the distribution. For the monsoon periods and assuming sea-salt  
11 composition in the grown spectra, only the broad mode was necessary to achieve the fit.

## 12 **5.5 Aerosol composition**

13 Sub-micron, non-refractory mass concentrations of four predominant aerosol composition  
14 fractions measured by the AMS - sulphate, organics, nitrate and ammonium - are plotted  
15 as relative composition by period in Figure 7, together with black carbon (BC)  
16 concentrations measured by the PSAP instrument.

17 Firstly, we note that due to the absence of industrial pollution sources and the  
18 generally very clean environment sampled in Darwin, very little ammonium or nitrate  
19 was sampled in any period, with vertical profiles generally varying around zero,  
20 reflecting random noise caused by ion counting statistics and a high background at the  
21 relevant mass-to-charge ratio in the mass spectrum. However, when averaged over many  
22 flights, statistically meaningful information could be obtained; even for the worst case of  
23 ammonium in the monsoon break, the standard error in the mean was less than 17%.

1 Significant concentrations of sulphate and organic material were sampled in most  
2 phases and show contrasting trends which provide useful information for discussions of  
3 air mass origin as well as local processes. The variation in organic aerosol loading  
4 between the different sampling periods follows the same broad trends as that for CO and  
5 fine mode aerosol. However, the correlation between organic mass and CO was strong  
6 only during the biomass burning periods. Such correlations are plotted in Figure 8 for a  
7 sample of typical flights in the biomass burning, pre-monsoon and monsoon break  
8 periods. No significant correlation was observed in the active or inactive monsoon  
9 phases. Each point in Figure 8 represents the simultaneous CO and AMS organic  
10 concentration, where CO data are averaged up to 30 seconds in line with the AMS time  
11 response. We see strong correlations ( $R^2 = 0.85, 0.65$ ) between CO and organic aerosol in  
12 the early burning phase flights (black and blue in Figure 8), with a clear reduction in  
13 dependence throughout the pre-monsoon and monsoon break phases ( $R^2 = 0.25, 0.08$   
14 respectively), illustrating the common burning sources in early flights and the  
15 independence of CO from sources of organic aerosol in the later clean phases. The  
16 absence of any significant correlation in the active and inactive monsoon phases ( $R^2 =$   
17  $0.01$ ) is expected in such maritime airmasses.

18 Throughout the burning and pre-monsoon phases, black carbon concentrations  
19 account for roughly 6% of the measured organic mass. Measurements made by *Ward et*  
20 *al.*, [1992, 1996] in the regional haze generated by African savanna and Brazilian fires  
21 measured around 3% BC in smouldering fires and ~15-20% in active flaming combustion  
22 with the exact aerosol makeup being highly dependant on the type of vegetation.  
23 However, we see that our measurements of BC in the burning season lie between these

1 two fire regimes suggesting that the air sampled over the Darwin area contained a mix of  
2 fire plumes generated in both active and smouldering fires further inland as might be  
3 expected. This is comparable with similar measurements of mixed air sampled by  
4 *Haywood et al.*, [2003], in the SAFARI 2000 experiment, where BC was observed to  
5 account for around 5% of the organic mass in burning plumes over Africa. Outside of the  
6 burning season, BC concentrations fall rapidly to ~1.5% in the active monsoon phase and  
7 falls below the limit of detection (~0.1% by mass) in the inactive monsoon phase and  
8 monsoon break.

9         The evolution in black carbon concentration and its vertical profile throughout the  
10 campaign is plotted in Figure 9, noting that PSAP black carbon measurements were not  
11 recorded above 1 km during flights in the mini-monsoon phase. Here, we see the same  
12 inter-seasonal evolution at all altitudes as for CO and fine aerosol discussed earlier, with  
13 a marked enhancement of soot particles and associated variability in the burning phase  
14 ( $0.4 \mu\text{g m}^{-3}$ , with extremes of up to  $1 \mu\text{g m}^{-3}$  at the 90th percentile), decreasing by around  
15 a factor of two in the pre-monsoon and dropping to zero in the monsoon phases, albeit at  
16 the limit of instrument sensitivity.

17         Analysis of AMS mass spectra during biomass burning periods offers some  
18 insights into the composition of the organic fraction and its transformation in the  
19 atmosphere. Figure 10a shows a mass spectrum of organic aerosol close to the source of  
20 a large fire. This spectrum is significantly different from that measured near a  
21 combustion aerosol source in an urban environment [e.g. *Canagaratna et al.*, 2004] and  
22 contains many more oxygenated species and evidence of monoacids such as  
23 levoglucosan, identified by unique peaks at  $m/z$  60 and 73 [*Alfarra et al.*, 2006]. Such



1 compounds are known to be directly emitted from biomass burning during the breakdown  
2 of lignin [*Jordan et al.*, 2006]. In contrast, a mass spectrum of biomass burning aerosol  
3 taken away from the source in the regional haze (Figure 10b) shows a marked change in  
4 relative composition with reduced relative abundance of larger mass fragments and a  
5 relative increase in  $m/z$  44, representative of a di-acid moiety. Similar enhancements  
6 have been seen in this fragment in aged continental aerosol in the northern hemisphere  
7 [*McFiggans et al.*, 2005]. These different mass spectra reflect a general trend in chemical  
8 fractionation of the organic mass as the biomass burning plumes age in the atmosphere.

9 An example mass spectrum of the organic fraction in clean air (Figure 10c)  
10 sampled later in the campaign again shows significant differences from aged continental  
11 pollution aerosol [e.g. *Zhang et al.*, 2005] and also from the biomass burning spectra  
12 shown in Figures 10a and 10b. The source of this organic aerosol is not clear, but  
13 potential origins may include biogenic activity or possibly material from the sea surface  
14 microlayer.

15 The organic mass fractions in both the biomass burning and clean periods are  
16 chemically distinctly different to those previously seen in anthropogenic-dominated  
17 midlatitude environments [e.g. *Zhang et al.*, 2005]. The sources, chemical nature and  
18 potential atmospheric implications of these organic aerosols will be discussed in future  
19 publications.

20 In contrast to the enhancement of the organic fraction, sulphate composition is  
21 only marginally higher in the burning season than the pre-monsoon, with a marked  
22 increase in terms of both median mass and associated variability in the active monsoon  
23 phase. This dramatic change in sulphate variability in the active monsoon follows trends

1 (of increased concentrations) observed in the coarse aerosol mode (recall Fig. 5b). It is  
2 highly likely that this enhanced sulphate is the result of oxidation of SO<sub>2</sub> by peroxide in  
3 solution, which can take place rapidly in cloud droplets near cloud base [*Ayers and*  
4 *Larson*, 1991, *Hegg*, 1992]. Should the pH rise sufficiently on droplet activation  
5 (become more neutral), S(IV) oxidation rates may be enhanced by ozone, as was  
6 observed by *Lowe et al.*, [1995], when cloud droplets were nucleated on relatively pH-  
7 neutral sea-salt aerosol. In summary, we deduce that enhanced sub-micron sulphate  
8 aerosol observed in the maritime monsoon air results from oxidative processing of SO<sub>2</sub> in  
9 cloud droplets. As was observed during ACE-1 [*Mari et al.*, 1998] di-methyl sulphide is  
10 the main source of sulphur in very clean, remote marine environments.

11         Interestingly, sulphate was much reduced and much less variable in the inactive  
12 monsoon, whilst coarse mode aerosol continued at high concentrations. Given the  
13 measurements available it is not possible to comment further on the exact mechanism  
14 leading to this observation as there are many possible reasons for reduced sulphate  
15 aerosol - such as reduced DMS emission, wet deposition further upwind, or a reduction in  
16 local cloud cover (and hence cloud processing) in the inactive monsoon. However,  
17 despite the reduction in overall loadings, the ratio of sulphate to ammonium was high in  
18 the inactive monsoon phase indicating that aerosols were more acidic than in other  
19 periods of the campaign; the ratio of sulphate mass to ammonium mass in those periods  
20 approached the molar ratio limit for molecular ammonium sulphate of 2.67, indicating  
21 that aerosols were generally pH neutral.

22         The nitrate fraction remained relatively small at around 1-4% of the total mass  
23 fraction considered here and is arguably smaller in the monsoon phases as might be

1 expected by its nature as a marker of continental pollution. However, such low signals  
2 within the AMS mass spectra, it is difficult to confidently state that the reported nitrate  
3 originates from ammonium nitrate, as is usual during continental sampling. Other species  
4 may be responsible for small amounts of reported nitrate, such as mineral or organic  
5 nitrates, or amines [*Allan et al.*, 2004b].

6

## 7 **7. Conclusions**

8 This paper describes the first measurements of gas phase species and aerosol size and  
9 composition in the tropical planetary boundary layer near Darwin, Australia as measured  
10 onboard aircraft operated as part of the ACTIVE campaign between November 2005 and  
11 February 2006.

12 Six periods of contrasting conditions in the background environment were  
13 identified during the campaign, which include a dry period of significant local, and more  
14 remote, land-clearance burning, followed by an intermediate period with no burning prior  
15 to a wet and subsequently dry monsoon phase and a later monsoon break. Of these, all  
16 periods except for the monsoon phases were characterised by daily isolated deep  
17 convective storms over the Darwin area and the nearby Tiwi Islands, capable of rapidly  
18 transporting boundary layer air to the TTL.

19 Carbon monoxide, fine mode aerosol, black carbon and organic aerosol loading  
20 all follow the same broad trends when comparing the different air mass periods. This  
21 mostly reflects influences from biomass burning with both fresh and secondary organic  
22 aerosols identified during the active burning phase. All were greatly reduced in the

1 monsoon phases which carried maritime air into the Darwin area. Ozone was highly  
2 variable but very low compared to northern hemispheric backgrounds at all times and  
3 broadly followed a similar evolution to CO and organic loadings. During the biomass  
4 burning period CO, aerosol fine mode number concentration and organic mass were  
5 positively and significantly correlated.

6 Coarse mode (super-micron) number concentration and fine-mode (sub-micron)  
7 sulphate aerosol loading were greatly enhanced in the active monsoon period indicating  
8 potentially significant sulphate aerosol production via aqueous phase S(IV) oxidation in  
9 cloud droplets activated on sea-salt aerosol lofted by mechanical disturbance of the ocean  
10 surface by high winds associated with the monsoon. Measured coarse mode spectra in the  
11 monsoon appear to agree well with the parameterisation by *Vignati et al.*, [2001], for sea-  
12 salt production in the range of wind speeds measured at this time. The sulphate aerosol  
13 component was reduced in the dry monsoon, possibly due to a reduction in cloud  
14 presence and hence cloud processes leading to sulphate production. However, high  
15 winds may have continued to loft large sea-salt particles, accounting in part for the large  
16 number of coarse mode aerosol at that time.

17 Nitrate and ammonium loadings were observed to be small and close to the limit  
18 of instrument sensitivity, although ammonium concentrations relative to sulphate after  
19 averaging indicates mostly pH-neutral aerosol for all but the monsoon phases where it  
20 may have been more acidic.

21 This dataset provides a reference of background conditions in the boundary layer  
22 across a wide range of meteorological and local conditions encountered in the Darwin  
23 region and offers valuable new information relating to the inflow to deep tropical

1 convective storms in the area and over the nearby Tiwi Islands. Modeling studies  
2 currently in progress are using the aerosol results reported here to calculate cloud  
3 condensation nuclei concentrations. Together with the gas phase measurements, these are  
4 used as input to models of deep convection which predict the composition of air lifted  
5 from the boundary layer to the TTL.

1 **Acknowledgements**

2

3 We thank NERC for funding the ACTIVE project and the NERC Airborne Research and  
4 Survey Facility (ARSF) for operational support of the Dornier-228 aircraft. This project  
5 would not have been possible without the extensive support of the Australian Bureau of  
6 Meteorology, in particular Peter May at the Bureau of Meteorology Research Centre,  
7 Melbourne and Lori Chappel at the Regional Forecasting Centre in Darwin. We also  
8 thank the RAAF base, Darwin, for hosting the aircraft and campaign base, and for their  
9 logistical support.

10

11 **References**

12

13 Agarwal, J. K., and G. J. Sem, Continuous Flow Single-Particle-Counting Condensation  
14 Nuclei Counter, *J. Aerosol Sci.*, 11, 4, 343–357, 1980/

15

16 Alfarra, M. R., Prevot, A. S. H., Szidat, S., et al., Identification of the mass spectral  
17 signature of organic aerosols from wood burning emissions, *Environ. Sci. Technol.*, in  
18 press, 2006.

19

20 Allan, J. D., J. L., Jimenez, P. I. Williams, M. E. Alfarra, K. N. Bower, J. T. Jayne, H.  
21 Coe, and D. R. Worsnop, Quantitative sampling using an Aerodyne Mass Spectrometer 1,

1 Techniques of data interpretation and error analysis, *J. Geophys. Res.*, 108(D3), 4090-  
2 4099, 2003.

3

4 Allan, J. D., H. Coe, K. N. Bower, M. E. Alfarra, A. E. Delia, J. L. Jimenez, A. M.  
5 Middlebrook, F. Drewnick, T. B. Onasch, M. R. Canagaratna, J. T. Jayne, and D. R.  
6 Worsnop, A generalised method for the extraction of chemically resolved mass spectra  
7 from Aerodyne aerosol mass spectrometer data, *J. Aerosol. Sci.*, 35, 909-922, 2004a

8

9 Allan, J. D., K. N. Bower, H. Coe, H. Boudries, J. T. Jayne, M. R. Canagaratna, D. B.  
10 Millet, A. H. Goldstein, P. K. Quinn, R. J. Weber, and D. R. Worsnop, Submicron  
11 aerosol composition at Trinidad Head, California, during ITCT 2K2: Its relationship with  
12 gas phase volatile organic carbon and assessment of instrument performance, *J. Geophys.*  
13 *Res.*, 109, 2004b

14

15 Ayers, G. P., and T. V. Larson, Numerical study of droplet size dependant chemistry in  
16 oceanic wintertime stratus cloud at southern mid-latitudes. *J. Atmos. Chem.*, 11, 143-167,  
17 1991

18

19 Baron, P. A. and K. Willeke, (Eds.), *Aerosol Measurement: Principles, Techniques, and*  
20 *Applications*, Van Nostrand Reinhold, New York, pp. 179-180, 1993.

21

1 Baumgardner, D., W. Strapp, and J. E. Dye, Evaluation of the forward Scattering  
2 Spectrometer Probe – Part II: Corrections for coincidence and dead-time losses, *J. Atmos.*  
3 *Oceanic Technol.*, 2, 626-632, 1985  
4  
5 Beswick, K. M., M. W. Gallagher, A. R. Webb, E. G. Norton, and F. Perry, Application  
6 of the Aventech AIMMS20AQ airborne probe for turbulence measurements during the  
7 Convective Storm Initiation Project, *Atmos. Chem. Phys. Discuss.*, 7, 3519–3555, 2007  
8  
9 Canagaratna, M. R., J. T. Jayne, D. A. Ghertner, S. Herndon, Q., Shi, J. L. Jimenez, P. J.  
10 Silva, P. I. Williams, T. Lanni, F. Drewnick, K. L. Demerjian, C. E. Kolb, and D. R>  
11 Worsnop, Chase studies of particulate emissions from in-use New York City vehicles,  
12 *Aerosol Sci. Technol.*, 38, 555-573, 2004  
13  
14 Carr, S.B., J. L. Gras, M. T. Hackett, and M. D. Keywood, Aerosol Characterisation in  
15 the Northern Territory of Australia during the Dry Season with an Emphasis on Biomass  
16 Burning, a report for the Defence Science and Technology Organisation, *DSTO-RR-0298*,  
17 Australia, 2005  
18  
19 Crook, N. A., Understanding Hector: The Dynamics of Island Thunderstorms, *Monthly*  
20 *Weather Review*, 129(6), 1550-1563, 2000  
21



1 Crosier, J., J. D. Allan, H. Coe, K. N. Bower, P. Formenti, and P. I. Williams, Chemical  
2 composition of summertime aerosol in the Po Valley (Italy), Northern Adriatic and Black  
3 Sea, Submitted to *Q. J. R. Met. Soc.*, 2006  
4  
5 Cross, E. S., J. G. Slowik, P. Davidovits, J. D. Allan, D. R. Worsnop, J. T. Jayne, D. K.  
6 Lewis, M. Canagaratna, and T. B. Onasch, Laboratory and ambient particle density  
7 determinations using light scattering in conjunction with aerosol mass spectrometry,  
8 *Aerosol Sci. Tech.*, in press, 2007.  
9  
10 Davies, D., Kumar, S., and Descloitres, J., Global fire monitoring using MODIS near-  
11 real-time satellite data. *GIM International*, 18(4):41-43, 2004  
12  
13 Dessler, A. E., The effect of deep tropical convection on the tropical tropopause layer, *J.*  
14 *Geophys. Res.* 107(D3), ACH 6-1 to ACH 6-5, 2002.  
15  
16 Edwards, D. P., L. K. Emmons, J. C. Gille, A. Chu, J.-L. Attié, L. Giglio, S. W. Wood, J.  
17 Haywood, M. N. Deeter, S. T. Massie, D. C. Ziskin, and J. R. Drummond, Satellite  
18 Observed Pollution From Southern Hemisphere Biomass Burning, *J. Geophys. Res.*, 111,  
19 D14312, doi:10.1029/2005JD006655, 2006.  
20  
21 Esler, J. G., D. G. H. Tan, P. H. Haynes, M. J. Evans, K. S. Law, P. Plantevin, and J. A.  
22 Pyle, Stratosphere-troposphere exchange: Chemical sensitivity to mixing, *J. Geophys.*  
23 *Res.*, 106(D5), 4717–4732, 2001

1

2 Fiebig, M., The tropospheric aerosol at midlatitudes - microphysics, optics, and climate  
3 forcing illustrated by the LACE 98 study, DLR-Forschungsbericht 2001-23, Cologne,  
4 Germany, 2001.

5

6 Giglio, L., J. Descloitres, C. O. Justice, and Y. J. Kaufman, An enhanced contextual fire  
7 detection algorithm for MODIS. *Remote Sensing of Environment*, 87:273-282, 2003

8

9 Gloudemans, A. M. S., M. C. Krol, J. F. Meirink, A. T. J. de Laat, G. R. van der Werf, H.  
10 Schrijver, M. M. P. van den Broek, and I. Aben, Evidence for long-range transport of  
11 carbon monoxide in the Southern Hemisphere from SCIAMACHY observations,  
12 *Geophys. Res. Lett.*, 33, L16807, doi:10.1029/2006GL026804, 2006

13

14 Gong, S. L., A parameterisation of sea-salt aerosol source function for sub and super-  
15 micron particles, *Global Biogeochem. Cycles*, 17(4), 1097, 2003

16

17 Hamilton, J. F., G. Allen, N. M. Watson, J. D. Lee, J. E. Saxton, A. C. Lewis, G.  
18 Vaughan, K. N. Bower, M. J. Flynn, J. Crozier, G. D. Carver, N. R. P. Harris, R. J.  
19 Parker, J. J. Remedios, and N. A.D. Richards, Observations of an Atmospheric Chemical  
20 Equator and its Implications for the Tropical Warm Pool Region, *J. Geophys Res.*, in  
21 press., 2007

22

1 Haywood, J. M., S. R. Osborne, P. N. Francis, A. Keil, P. Formenti, M. O. Andreae, and  
2 P. H. Kaye, The mean physical and optical properties of regional haze dominated by  
3 biomass burning aerosol measured from the C-130 aircraft during SAFARI 2000, *J.*  
4 *Geophys. Res.*, 108(D13), 8473, doi:10.1029/2002JD002226, 2003

5

6 Heintzenberg, J., D. C. Covert, and R. van Dingenen, Size distribution and chemical  
7 composition of marine aerosols: a compilation and review, *Tellus B*, 52(4), p.1104, 2000

8

9 Hegg, D. A., Modeling the effects of heterogeneous cloud chemistry on the marine  
10 particle size distribution. *J Geophys. Res.*, 97(D12), 12,927-12,933, 1992

11

12 IPCC: *Climate change 2001: The Scientific Basis. Contribution of Working Group I to*  
13 *the Third Assessment Report of the Intergovernmental Panel on Climate Change*  
14 [Houghton, J. T., Y. Ding, D. J. Griggs, M. Noguer, P. J. van der Linden, X. Dai, K.  
15 Maskell and C. A. Johnson (eds.)]. Cambridge University Press, Cambridge, United  
16 Kingdom and New York, NY, USA, 881pp, 2001

17

18 Jayne, J. T., D. C. Leard, X. F. Zhang, P. Davidovits, K. A. Smith, C. E. Kolb, and D. R.  
19 Worsnop, Development of an aerosol mass spectrometer for size and composition  
20 analysis of submicron particles, *Aeros. Sci. Tech.*, 33, 1, 49-70, 2000

21

1 Jimenez, J. L., J. T. Jayne, Q. Shi, C. E. Kolb, D. R. Worsnop, I. Yourshaw, J. H.  
2 Seinfeld, R. C. Flagan, X. Zhang, K. A. Smith, J. W. Morris, and P. Davidovits, Ambient  
3 aerosol sampling using the Aerodyne Mass Spectrometer, *J. Geophys. Res.*, 108(D7),  
4 8425-8437. doi:10.1029/2001JD001213, 2003  
5  
6 Jordan, T. B., A. J. Seen, and G. E. Jacobsen, Levoglucosan as an atmospheric tracer for  
7 woodsmoke, *Atmos Env*, 40, 5316–5321, 2006  
8  
9 Kondo, Y., K. Ko, M. Koike, S. Kawakami, and T. Ogawa, Preface to special section on  
10 biomass burning and lightning experiment (BIBLE), *J. Geophys. Res.*, 108(D3), 8397,  
11 doi:10.1029/2002JD002401, 2003  
12  
13 Lefohn A.S., S. J. Oltmans, T. Dann, and H. B. Singh, Present-day variability of  
14 background ozone in the lower troposphere. *J. Geophys. Res.*, 106(D9), 9945-9958, doi:  
15 10.1029/2000JD900793, 2001  
16  
17 Liley, J. B., D. Baumgardner, Y. Kondo, K. Kita, D. R. Blake, M. Koike, T. Machida, N.  
18 Takegawa, S. Kawakami, T. Shirai, and T. Ogawa, Black carbon in aerosol during  
19 BIBLE B, *J. Geophys. Res.*, 107, 8399, doi:10.1029/2001JD000845, [printed 108(D3),  
20 2003], 2002.  
21

1 Liu Y. and P. H. Daum, The effect of refractive index on size distributions and light  
2 scattering coefficients derived from optical particle counters, *J. Aero. Sci.*, 31, 8, 945-  
3 957, 2000  
4  
5 Lohmann, U., and J. Feichter, Global indirect aerosol effects: a review, *Atmos. Chem.*  
6 *Phys.*, 5, 715-737, 2005  
7  
8 Lowe, J. A., M. H. Smith, S. L. Clegg, and C. D. O'Dowd, Influence of sub-micron sea-  
9 salt aerosols on sulphate production in marine clouds. NERC Report *GR9/1020*, NERC,  
10 Swindon, 2005  
11  
12 Manton, M. J., and J. L. McBride, Recent research on the Australian Monsoon, *J. Met.*  
13 *Soc. Japan*, 70, 275-285, 1992  
14  
15 Mari, C., K. Suhre, T. S. Bates, J. E. Johnson, R. Rosset, A. R. Bandy, F. L. Eisele, R. L.  
16 Mauldin, D. C. Thornton, Physico-chemical modeling of the first aerosol  
17 Characterization Experiment (ACE 1) lagrangian B. 2. DMS emission, transport and  
18 oxidation at the mesoscale: First Aerosol Characterization Experiment (ACE 1), *J.*  
19 *Geophys. Res.*, 103(D13), 16457-16473, 1998  
20  
21 McFiggans, G., P. Artaxo, U. Baltensperger, H. Coe, M. C. Facchini, G. Feingold, S.  
22 Fuzzi, M. Gysel, A. Laaksonen, U. Lohmann, T. F. Mentel, D. M. Murphy, C. D.

1 O'Dowd, J. R. Snider, and E. Weingartner, The effect of physical and chemical aerosol  
2 properties on warm cloud droplet activation, *Atmos. Chem. Phys.*, 6, 2593-2649, 2006  
3  
4 McFiggans, G., M. R. Alfarra, J. Allan, K. N. Bower, H. Coe, M. Cubison, D. Topping,  
5 P. I. Williams, S. Decesari, C. Facchini, and S. Fuzzi, Simplification of the representation  
6 of the organic component of atmospheric particulates, *Faraday Discuss.*, 130, 341-362,  
7 2005.  
8  
9 O'Dowd, C. D., M. H. Smith, I. E. Consterdine, and J. A. Lowe, Marine aerosol, sea-  
10 salt, and the marine sulphur cycle: A review, *Atmos. Env.*, 31(1), 73-80, 1997  
11  
12 Petzold, A., M. Fiebig, H. Flentje, A. Keil, U. Leiterer, F. Schröder, A. Stifter, M.  
13 Wendisch, and P. Wendling, Vertical variability of aerosol properties observed at a  
14 continental site during LACE 98, *J. Geophys. Res.*, 107, LAC 10-1 - LAC 10-18, doi  
15 10.1029/2001JD001043, 2002  
16  
17 Pruppacher, H. P. and J. D. Klett, (Eds.), *Microphysics of clouds and precipitation*, 26pp.,  
18 Kluwer Academic Press, 1997.  
19  
20 Russell-Smith, J., G. Allan, R. Thackway, T. Rosling, and R. Smith, Fire Management  
21 and Savannah Landscapes in Northern Australia, in *Fire and Sustainable Agricultural and*  
22 *Forestry Development in eastern Indonesia and northern Australia*, *ACIAR Proceedings*

1 No. 91, Australian Centre for International Agricultural Research, Canberra, pp 95-101,  
2 2000  
3  
4 Russell-Smith, J., C. Edwards, and G. D. Cook, Reliability of biomass burning estimates  
5 from savanna fires: Biomass burning in northern Australia during the 1999 Biomass  
6 Burning and Lightning Experiment B field campaign, *J. Geophys. Res.*, 108, D3, 8405,  
7 2003  
8  
9 Saxton, J. E., A. C. Lewis, J. H. Kettlewell, M. Z. Ozel, F. Gogus, Y. Boni, S. O. U.  
10 Korogone, D. Serça, Isoprene and monoterpene emissions from secondary forest in  
11 northern Benin, *Atmos. Chem. Phys. Disc*, 7, 4981-5012, 2007  
12  
13 Sherwood, S. C., and A. E. Dessler, On the control of stratospheric humidity, *Geophys.*  
14 *Res. Lett.*, 27, 2513-2516, 2000  
15  
16 Staudt, A. C., D. J. Jacob, D. Bachiochi, T. N. Krishnamurtiand, G. W. Sachse, and J.  
17 Logan, Continental sources, transoceanic transport, and inter-hemispheric exchange of  
18 carbon monoxide over the Pacific, *J. Geophys. Res.*, 106, D23, 32571-32590, 2001  
19  
20 Stohl, A., et al., Stratosphere-troposphere exchange: A review, and what we have learned  
21 from STACCATO, *J. Geophys. Res.*, 108(D12), 8516, doi:10.1029/2002JD002490, 2003  
22

1 Takegawa, N., Y. Miyazaki, Y. Kondo, Y. Komazaki, T. Miyakawa, J. L. Jimenez, J. T.  
2 Jayne, D. R. Worsnop, J. D. Allan, and R. J. Weber, Characterization of an Aerodyne  
3 Aerosol Mass Spectrometer (AMS): Intercomparison with other aerosol instruments,  
4 *Aerosol Sci. Technol.*, 39, 760-770, 2005  
5  
6 Topping, D. O., G. B. McFiggans, and H. Coe, A curved multi-component aerosol  
7 hygroscopicity model framework: 2 – Including organics, *Atmos. Chem. Phys.*, 5, 1223-  
8 1242, 2005  
9  
10 Ward, D. E., R. A. Susott, J. B. Kaufman, R. E. Babbitt, D. L. Cummings, B. Dias, B. N.  
11 Holben, Y. J. Kaufman, R. A. Rasmussen, and A. W. Setzer, Smoke and fire  
12 characteristics for cerrado and deforestation burns in Brazil: Base-B experiment, *J.*  
13 *Geophys. Res.*, 97, 14,601 – 14,619, 1992  
14  
15 Ward, D. E., W. M. Hao, R. A. Susott, R. E. Babbitt, R. W. Shea, J. B. Kaufman, and C.  
16 O. Justice, Effect of fuel composition on combustion efficiency and emission factors for  
17 African savanna ecosystems, *J. Geophys. Res.*, 101, 23,569– 23,576, 1996  
18  
19 Vaughan, G., C. Schiller, A. R. MacKenzie, K. N. Bower, T. Peter, H. Schlager, N. R. P.  
20 Harris and P. T. May, Studies in a natural laboratory: High-altitude aircraft measurements  
21 around deep tropical convection, *BAMS*, in press, 2007  
22



1 Vignati, E., G. de Leeuw, and R. Berkowicz, Modeling coastal aerosol transport and  
2 effects of surf-produced aerosols on processes in the marine atmospheric boundary layer,  
3 *J. Geophys. Res.*, 106(D17), 20,225–20,238, 2001

4

5 Zhang, Q., M. R. Alfarra, D. R. Worsnop, J. D. Allan, H. Coe, M. R. Canagaratna, and J.  
6 L. Jimenez, Deconvolution and Quantification of Hydrocarbon-like and Oxygenated  
7 Organic Aerosols Based on Aerosol Mass Spectrometry, *Environ. Sci. Technol.*, 39,  
8 4938-4952, 2005

1 Figure 1 MODIS-derived fire maps of the Australasian region integrated between: 17-30  
2 Nov 2005 (top); 7-12 Dec 2005 (middle), and 21-30 Jan 2005 (bottom). Images courtesy  
3 of MODIS Rapid Response Project at NASA/GSFC.

4

5 Figure 2 Dornier aerodynamic inlet configuration (Figure courtesy of Andreas Petzold,  
6 Deutsche Zentrum für Luft und Raumfahrt)

7

8 Figure 3 Five-day ECMWF back-trajectories initiated from Darwin (130.9 E, -12.41 S) at  
9 700 mb and 900 mb at 0600 UTC (1530 local time) for every day within each time period  
10 indicated.

11

12 Figure 4 Average boundary layer profiles of carbon monoxide and ozone, colour-coded  
13 by time period as indicated. The box-centre denotes the median concentration; box edges  
14 the upper and lower quartiles; and extremities the 10<sup>th</sup> and 90<sup>th</sup> percentile concentrations.  
15 Note that no measurements were made above 2 km in the active monsoon period.

16

17 Figure 5 Vertical profiles of aerosol total number concentration calculated from: a) ASP;  
18 and b) FSSP integrated over 0.3 to 2.5  $\mu\text{m}$ ; and 2 to 32  $\mu\text{m}$  respectively. Box centre  
19 denotes the median; box edges the upper and lower quartiles; and extremities the 10<sup>th</sup> and  
20 90<sup>th</sup> percentiles. Note that measurements were not recorded above 2 km in the active  
21 monsoon period.

1

2 Figure 6 Composite median aerosol size spectra (normalised for size-bin width), colour-  
3 coded by time period as indicated and measured by the ASP (0.22-1.8  $\mu\text{m}$ ) and the FSSP  
4 (2.0 – 32  $\mu\text{m}$ ) showing a) Number concentration; b) Surface area; c) Volume; d) Number  
5 concentration assuming chloride growth factor; e) Surface area assuming chloride growth  
6 factor; and f) Volume assuming chloride growth factor.

7

8 Figure 7 Pie charts of relative aerosol composition colour-coded as indicated for each  
9 time period of ACTIVE. Mass concentrations are quoted as the mean ( $\mu\text{g cm}^{-3}$ ) over all  
10 flights within each period, together with the standard error.

11

12 Figure 8 Correlations between measured carbon monoxide and organic aerosol  
13 composition over the course of ACTIVE colour-coded by flight number as indicated.  
14 Periods corresponding to each flight are: SD06, AD08 and AD09 – Biomass burning;  
15 AD11 – Pre-monsoon; AD26 – Monsoon break.

16

17 Figure 9 Vertical profile of black carbon (soot) measured by the PSAP, colour-coded by  
18 time period. Box centre denotes the median; box edges the upper and lower quartiles; and  
19 extremities the 10<sup>th</sup> and 90<sup>th</sup> percentiles. Note that measurements were not recorded above  
20 2 km in the active monsoon or above 1 km in the mini-monsoon period.

21

- 1 Figure 10 Typical mass spectra recorded by the AMS normalised to nitrate equivalent
- 2 mass concentration for flight: a) SD05 - A flight in the plume of an active inland scrub
- 3 fire in the mini-monsoon period; b) AD04 - A flight through haze layer in the biomass
- 4 burning period; and c) AD25 - A clean flight in the monsoon break

1

Instrument	Size Range (diameter)	Technique	Reference/Company
UHSAS	0.055 - 0.8 $\mu\text{m}$	Optical scattering	Droplet Measurement Technologies Inc
Grimm 1.108	0.3 – 25 $\mu\text{m}$	Optical counter	Grimm Technologies Inc
ASP	0.21 – 4.5 $\mu\text{m}$	Optical scattering	Droplet Measurement Technologies Inc
FSSP	0.5 – 32 $\mu\text{m}$	Optical scattering	<i>Baumgardner et al.</i> , [1985]
TSI-1301D	> 10 nm	Condensational growth	<i>Argarwal and Sem</i> , [1980]
PSAP	-	Integration plate	Radiancance Research Inc
AMS	0.04 – 0.7 $\mu\text{m}$	70 eV Quadrupole mass spectrometry	<i>Jayne et al.</i> , [2000]
Filters	-	Particle deposition	

2  
3

**Table 1 Aerosol instruments onboard the Dornier aircraft with measured size ranges given where appropriate. See text for a further description of each instrument.**

1

Instrument	Technique	Gases	Reference/Company
Aerolaser AL5002	Fluorescence	CO	Aerolaser Inc
2B Technologies 202 ozone analyser	UV absorption	O <sub>3</sub>	2B Technologies
Automatic tube sampler	Absorbent trapping and GC-MS	C5-C10 aliphatics, aromatics monoterpenes, OVOCs	University of York
Miniature GC	Gas Chromatography	Halocarbons (Cl, Br, I)	<i>Robinson et al.</i> , [2000]

2

**Table 2 Gas phase instrumentation and measurement technique on the Dornier aircraft.**

1

Date	Flight Label	Primary Mission	Date	Flight Label	Primary Mission
8 Nov 2005	TD01	Instrument test	22 Jan 2006	AD15	Monsoon Inflow (Inland) <sup>†</sup>
13 Nov 2005	TD02	Test/Tiwi survey	25 Jan 2006	AD16	Tiwi Survey <sup>†</sup>
15 Nov 2005	AD03	Tiwi survey	26 Jan 2006	SD17	Inland Survey
16 Nov 2005	AD04	Tiwi survey*	27 Jan 2006	SD18	Inland Survey <sup>†</sup>
19 Nov 2005	SD05	Tiwi Survey*	30 Jan 2006	SD19	Northern Hemisphere Plume
23 Nov 2005	SD06	Inland Survey	1 Feb 2006	SD20	Survey to Alice Springs
24 Nov 2005	SD07	Inland Survey	2 Feb 2006	SD21	Survey (return to Darwin)
28 Nov 2005	AD08	Tiwi Survey	3 Feb 2006	SD22	Northern Hemisphere Plume
30 Nov 2005	AD09	Tiwi Survey*	6 Feb 2006	AD23	Tiwi Survey <sup>†</sup>
1 Dec 2005	AD10	Tiwi Survey	8 Feb 2006	AD24	Tiwi Survey <sup>†</sup>
4 Dec 2005	AD11	Tiwi Survey	9 Feb 2006	AD25	Tiwi Survey
5 Dec 2005	AD12	Inland Survey	10 Feb 2006	AD26	Tiwi Survey <sup>†</sup>
19 Jan 2006	TD13	Test/Tiwi Survey	12 Feb 2006	AD27	Inland survey
20 Jan 2006	AD14	Monsoon inflow (Tiwis)	14 Feb 2006	AD28	Instrument Intercomparison

2

**Table 3 A summary of Dornier-228 missions throughout ACTIVE. First letter of flight label denotes mission type (T=test, A=convective inflow mission, S=wider area background survey), whilst the second letter signifies the Dornier aircraft.**

3

4

5

\*Coincident with SCOUT-O3 mission; †Coincident with TWP-ICE mission

1

Period	Prevailing influence	Flights within period
13 – 19 Nov + 25 – 30 Nov	Biomass Burning	TD02 – SD05 + AD08-AD09
20 – 24 Nov	Mini-Monsoon	SD06 – SD07
30 Nov – 5 Dec	Pre-Monsoon	AD10 – AD12
14 Jan – 22 Jan	Active Monsoon	TD13 – AD15
25 Jan – 27 Jan	Inactive Monsoon	AD16 – SD18
4 Feb – 14 Feb	Monsoon Break	AD23 – AD28

2

**Table 4 Periods of meteorological contrast during ACTIVE flight operations**



1

Period	CO / ppbv							Ozone / ppbv						
	Mean	Std. Dev	Med	10%	25%	75%	90%	Mean	Std. Dev	Med	10%	25%	75%	90%
Biomass Burning	112.3	20.7	102.4	80.8	88.6	116.4	136.4	25.3	3.6	24.2	16.3	20.0	29.7	35.5
Mini-monsoon	98.1	7.9	89.0	79.6	84.5	93.3	98.0	26.3	2.8	25.5	17.3	20.7	31.0	36.4
Pre-Monsoon	88.9	4.1	86.4	75.8	80.5	92.3	96.7	25.1	2.7	24.7	18.0	21.2	28.8	33.3
Active monsoon	69.2	3.3	67.9	58.0	62.4	74.2	77.7	20.0	3.1	19.8	13.0	16.4	23.0	25.8
Inactive monsoon	52.3	8.5	51.5	43.2	45.5	57.9	62.8	17.5	3.1	17.8	10.7	14.0	20.2	24.6
Monsoon break	59.4	2.6	58.5	50.7	54.0	64.2	69.5	21.9	3.2	21.3	13.8	17.1	26.3	31.2

2 **Table 5 Concentration statistics for carbon monoxide and ozone within each meteorological period**  
3 **averaged for all altitudes greater than 100m. Concentrations are quoted in parts per billion by**  
4 **volume.**

1

Species	Biomass Burning			Mini-Monsoon			Pre-monsoon		
	Median	Max	Min	Median	Max	Min	Median	Max	Min
ethyl benzene	33	198.6	4.9	20	44.5	3.4	37	388.3	3.7
m + p xylene	85	336.7	12.1	41	106.8	1.7	81	185.8	8.0
o-xylene	36	215.8	6.5	21	54.0	2.1	39	97.5	3.0
nonane	61	264.6	12.4	8	10.2	6.4	96	259.5	31.1
isopropyl benzene	5	45.3	0.2	3	9.4	0.4	7	40.8	1.1
3-ethyltoluene	29	183.2	3.2	16	44.4	0.3	31	61.7	6.3
1,3,5-trimethyl	14	115.3	1.8	8	25.0	0.2	18	35.3	3.6
1,2,4-trimethyl-	34	172.4	2.5	17	45.7	<LOD	35	77.2	7.0
1,2,3-trimethyl	12	136.7	1.0	9	24.2	<LOD	22	53.0	3.9
propyl benzene	12	87.4	1.8	6	38.6	0.6	13	47.9	2.3
Species	Active Monsoon			Inactive Monsoon			Monsoon Break		
	Median	Max	Min	Median	Max	Min	Median	Max	Min
ethyl benzene	21	65.9	2.0	24	517.7	1.3	14	101.5	0.2
m + p xylene	37	155.9	3.6	45	228.7	1.5	26	154.1	<LOD
o-xylene	20	74.4	3.4	29	299.8	<LOD	13	101.5	0.1
nonane	31	136.3	9.5	38	15.4	<LOD	10	54.2	0.3
isopropyl benzene	4	9.4	0.9	2	52.8	0.2	3	29.3	<LOD
3-ethyltoluene	17	51.7	1.2	4	90.9	0.8	10	38.5	<LOD
1,3,5-trimethyl	7	27.4	0.9	13	103.2	1.0	6	20.3	<LOD
1,2,4-trimethyl-	12	88.3	0.5	20	252.8	1.8	7	37.7	<LOD
1,2,3-trimethyl	5	17.4	0.7	10	119.5	0.2	2	23.0	<LOD
propyl benzene	5	17.9	0.8	6	53.0	<LOD	3	20.6	<LOD

2 **Table 6 Volatile organic carbonaceous gas concentration statistics for each meteorological regime**  
3 **during ACTIVE. All concentrations are given in parts per trillion by volume (pptv)**

1

		Burning	Mini-Monsoon	Pre-monsoon	Active Monsoon	Inactive Monsoon	Monsoon Break
Fine Mode 1	$N_{tot}$	$203 \pm 65$	$203 \pm 57$	$102 \pm 41$	$272 \pm 845$	$172 \pm 619$	$175 \pm 258$
	$\ln(\sigma_g)$	$0.23 \pm 0.04$	$0.24 \pm 0.04$	$0.24 \pm 0.05$	$36.6 \pm 40.1$	$0.58 \pm 0.48$	$0.28 \pm 0.13$
	$D_g$	$0.28 \pm 0.03$	$0.29 \pm 0.02$	$0.27 \pm 0.03$	$0.18 \pm 0.18$	$0.13 \pm 0.21$	$0.21 \pm 0.09$
Fine Mode 2	$N_{tot}$	$7.14 \pm 14.81$	$49.7 \pm 161.5$	$5.64 \pm 16.02$	$110 \pm 3314$	$0.62 \pm 38.3$	$102 \pm 1720$
	$\ln(\sigma_g)$	$0.73 \pm 0.22$	$0.81 \pm 0.25$	$0.90 \pm 0.43$	$1.04 \pm 2.02$	$0.78 \pm 4.16$	$1.09 \pm 1.27$
	$D_g$	$0.2 \pm 0.3$	$0.13 \pm 0.21$	$0.21 \pm 0.41$	$0.03 \pm 0.53$	$0.23 \pm 6.36$	$0.03 \pm 0.26$
Coarse Mode	$N_{tot}$	$0.19 \pm 0.05$	$0.14 \pm 1.61$	$0.15 \pm 0.04$	$1.61 \pm 0.26$	$1.61 \pm 0.27$	$0.44 \pm 0.14$
	$\ln(\sigma_g)$	$0.51 \pm 0.06$	$0.53 \pm 0.06$	$0.54 \pm 0.06$	$0.59 \pm 0.03$	$0.53 \pm 0.02$	$0.54 \pm 0.07$
	$D_g$	$3.61 \pm 0.35$	$3.53 \pm 0.38$	$3.21 \pm 0.35$	$4.40 \pm 0.32$	$4.20 \pm 0.26$	$3.04 \pm 0.45$

2 **Table 7 Lognormal fit parameters and confidences for median aerosol spectra within each**  
3 **meteorological period of ACTIVE. The uncertainty represents the upper and lower 95% confidence**  
4 **level. The fine and coarse mode parameters refer to spectra measured by the ASP and FSSP**  
5 **respectively.**

1 Table 8

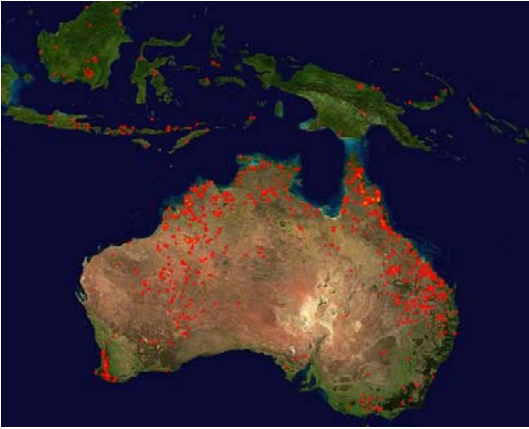
2

	Active Monsoon	Inactive Monsoon	Monsoon Break
$N_{tot}$	$370 \pm 1091$	$45.2 \pm 52.0$	$473 \pm 3048$
$\ln(\sigma_g)$	$0.53 \pm 0.19$	$0.45 \pm 0.11$	$0.62 \pm 0.40$
$D_g$	$0.34 \pm 0.37$	$0.58 \pm 0.29$	$0.21 \pm 0.52$

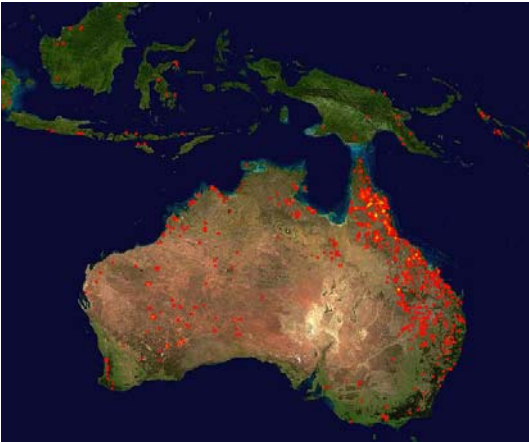
3 **Table 8 Lognormal fit parameters and confidences for median fine mode aerosol spectra with pure**  
4 **chloride growth factors applied for the monsoon and monsoon-break phases of ACTIVE.**  
5 **Uncertainty represents the upper and lower 95% confidence level.**

1 Figure 1

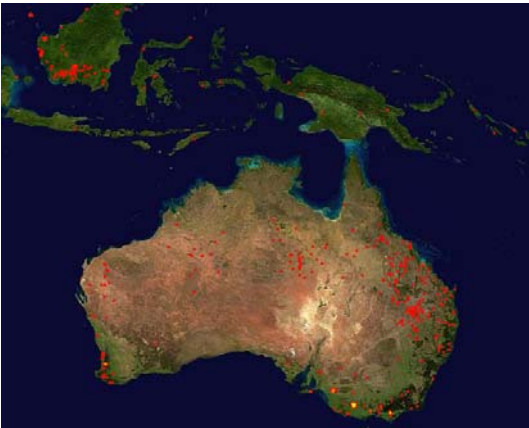
2



3



4

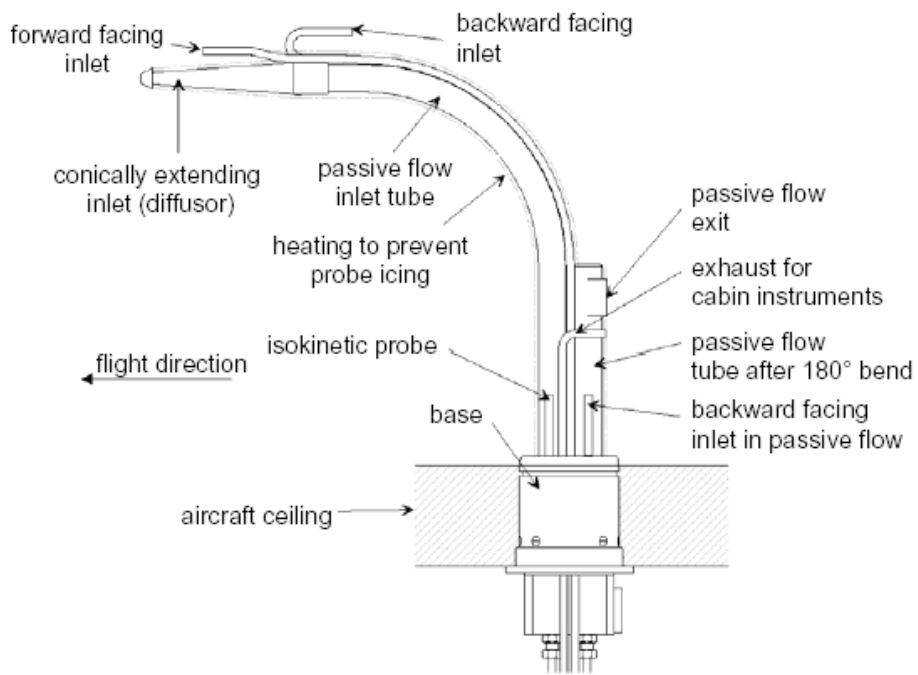


5

6

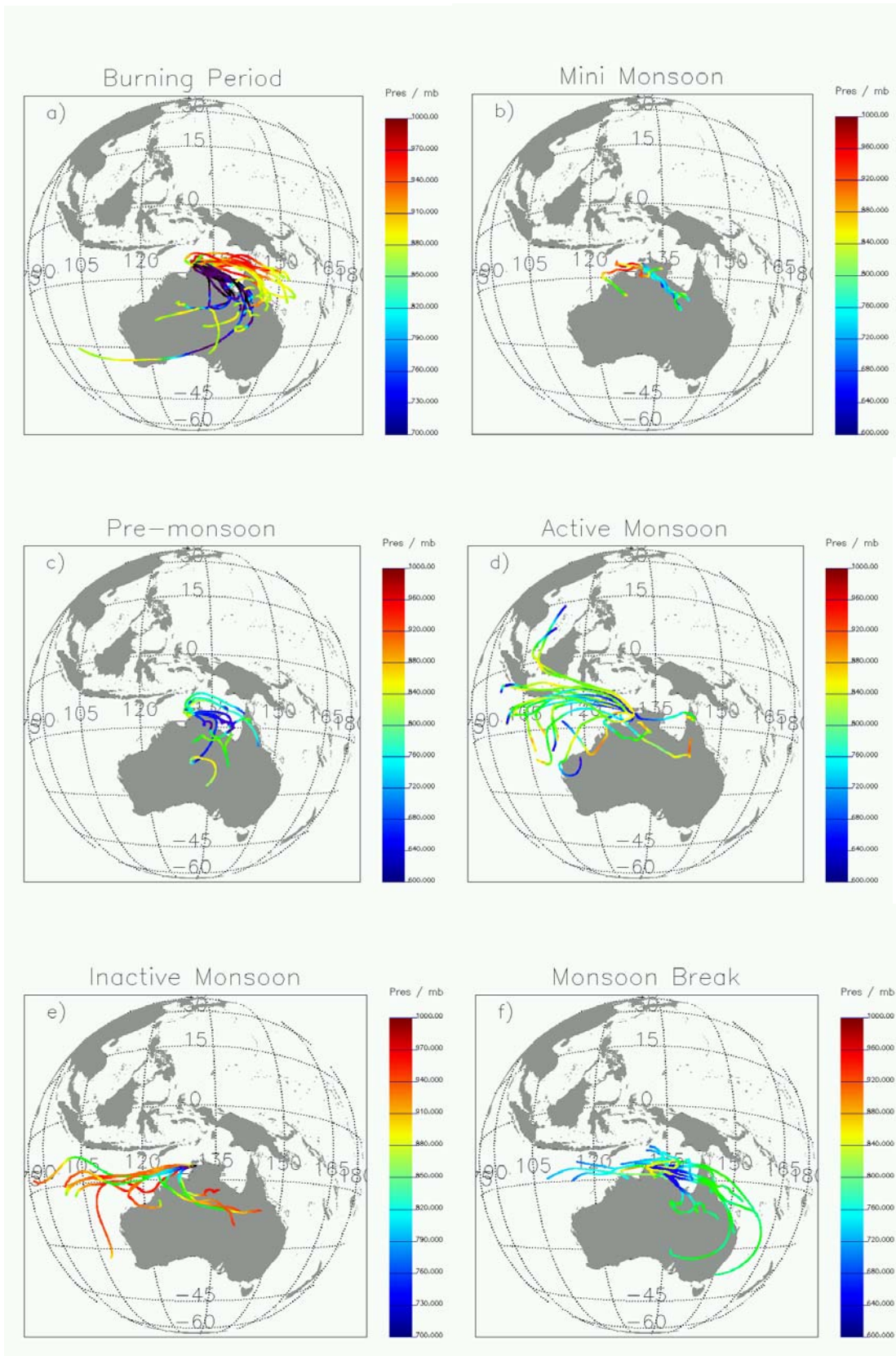
1 Figure 2

2



3

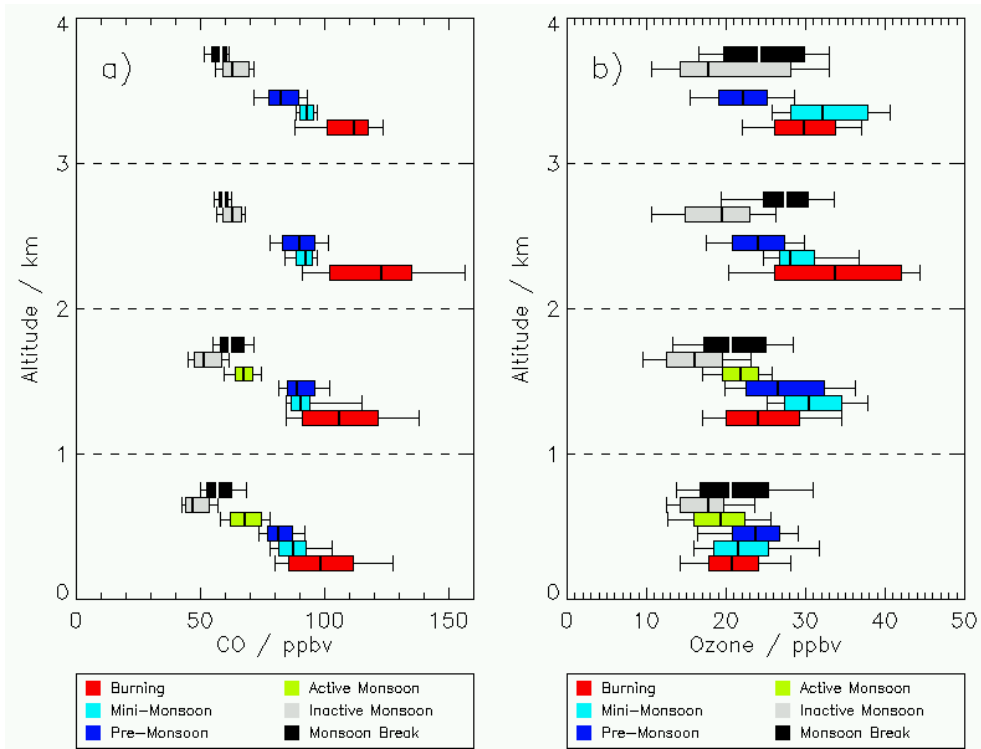
1 **Figure 3**



1

2 Figure 4

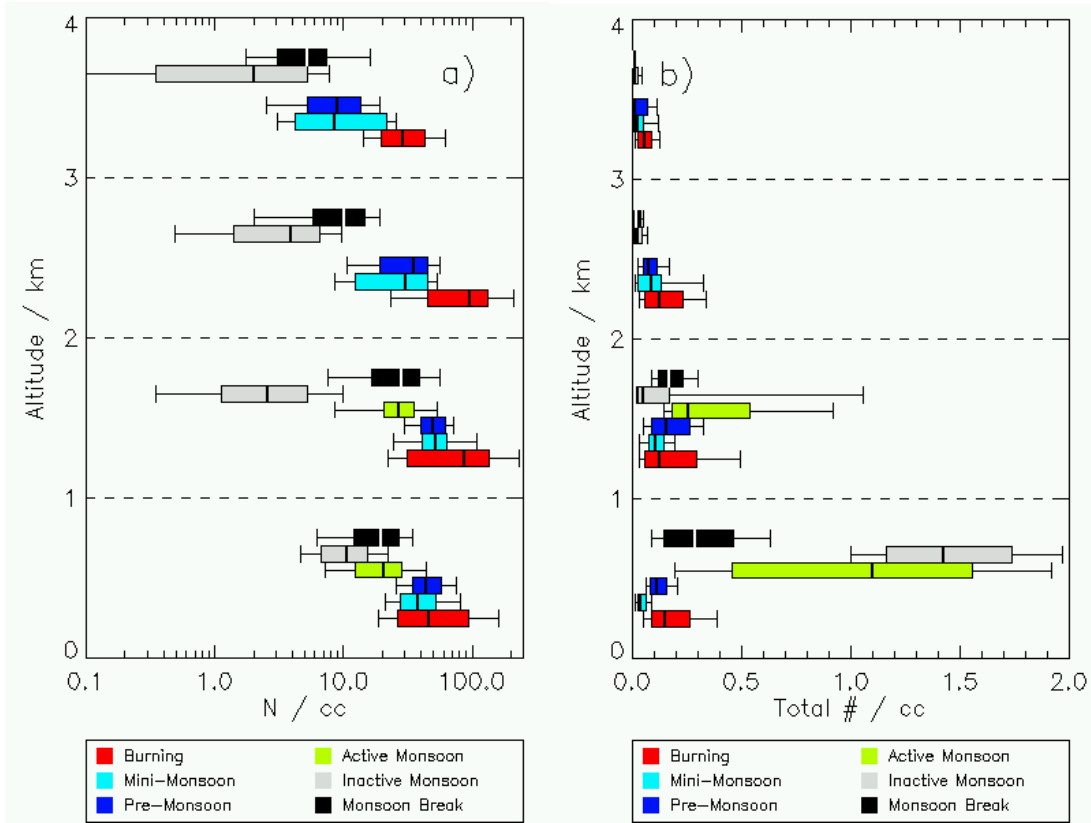
3



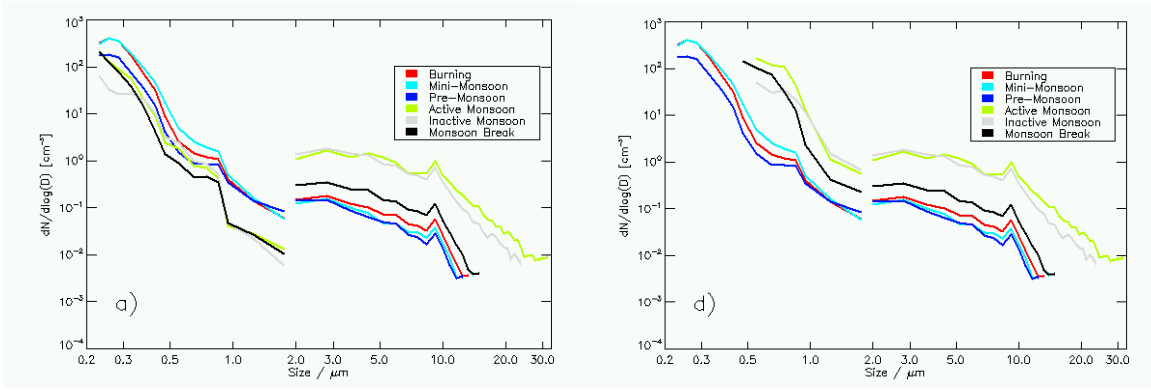
4



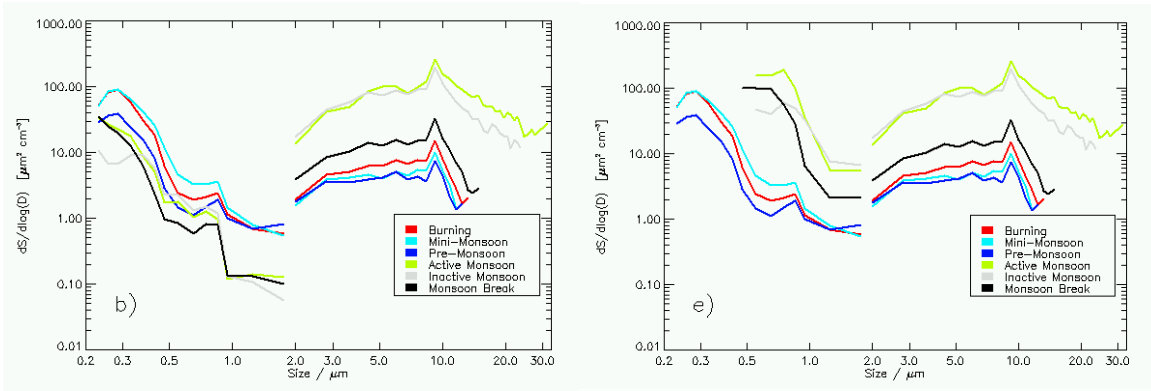
1 Figure 5  
 2



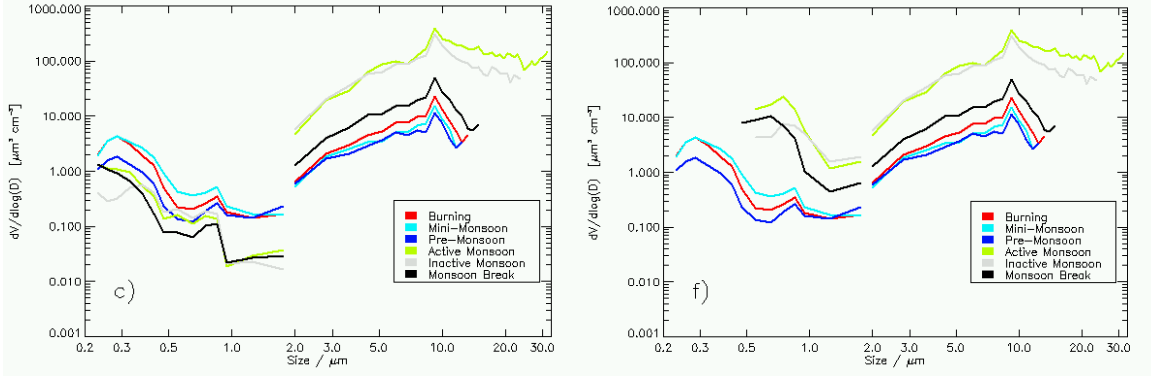
3  
 4  
 5  
 6  
 7



1



2



3

4

5

6

Figure 6

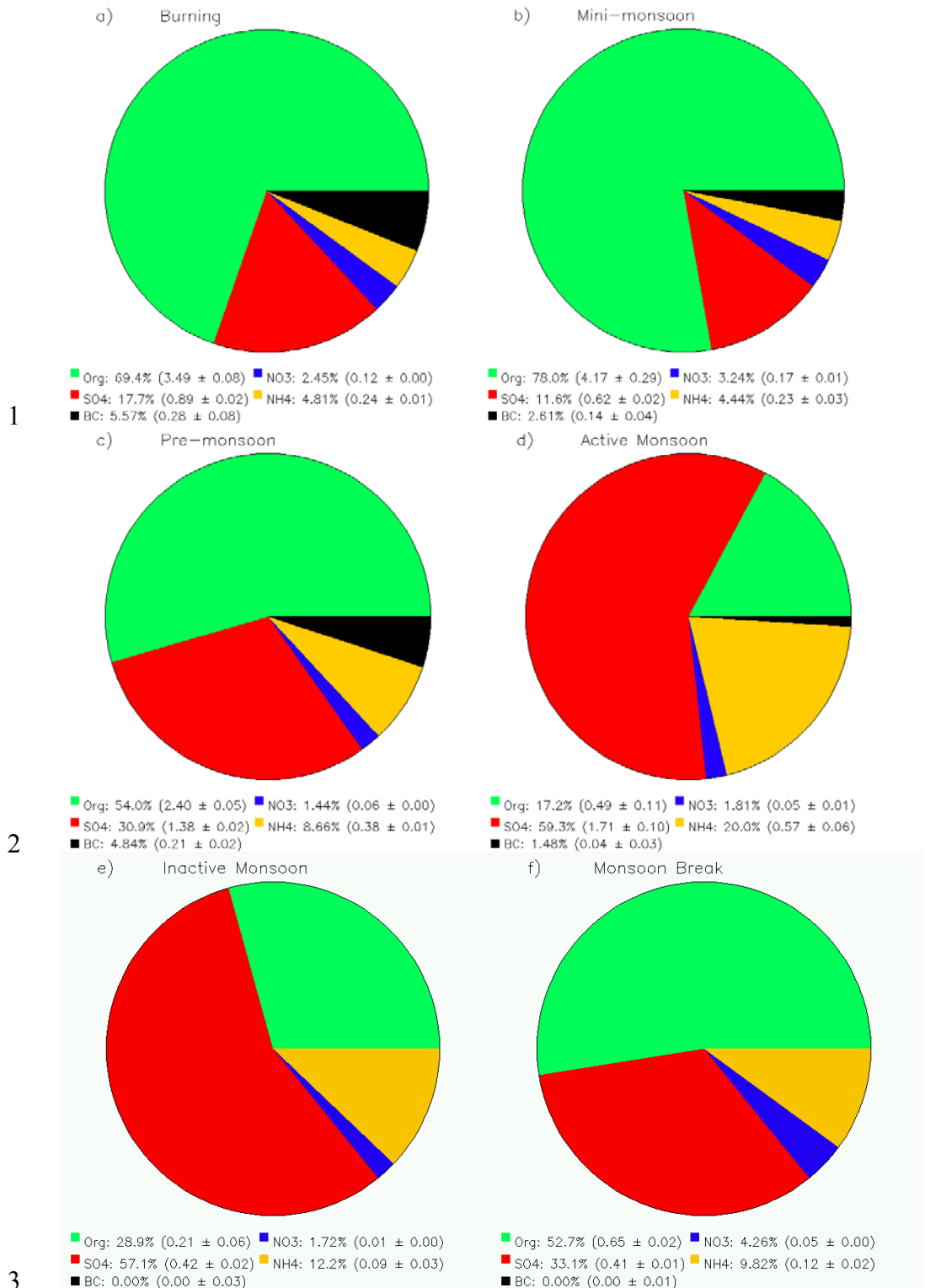
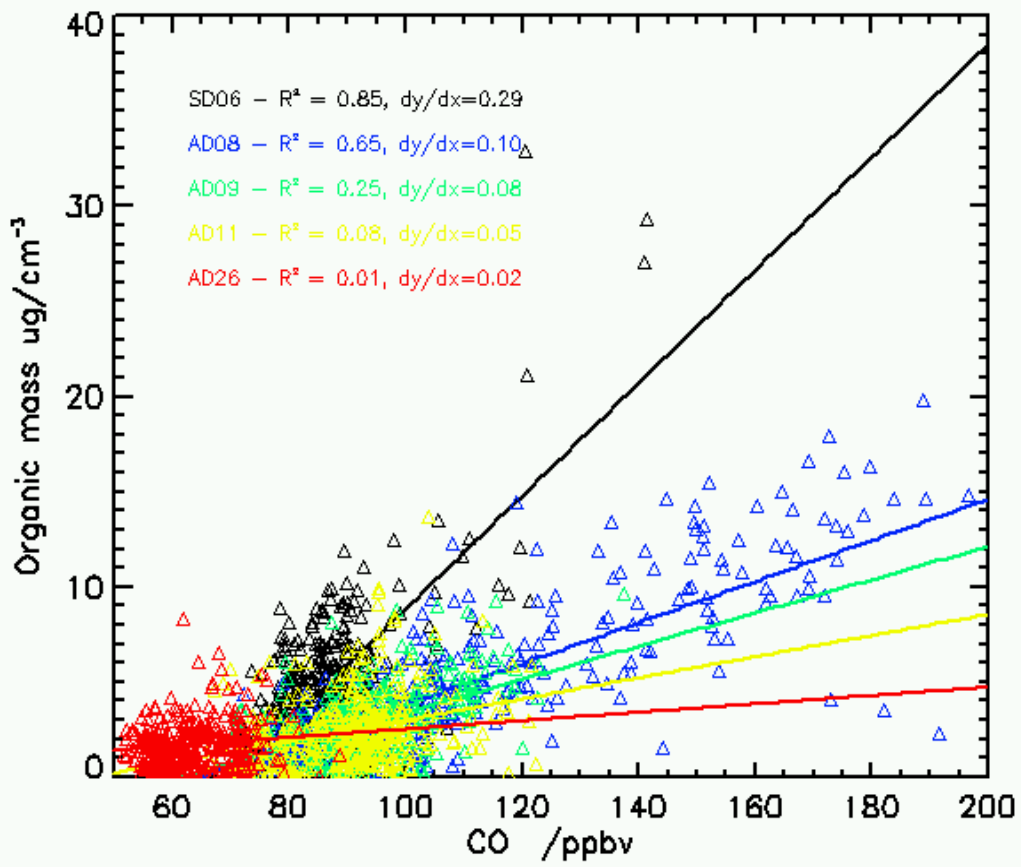
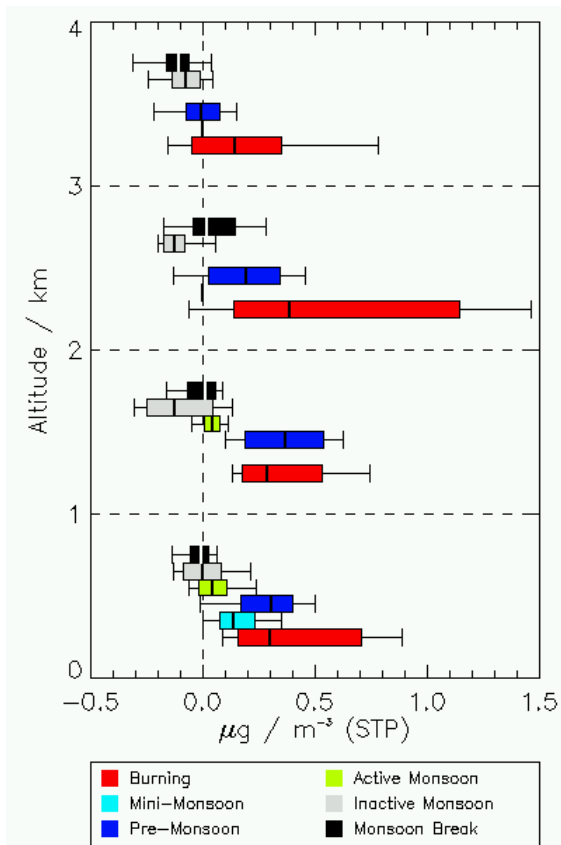


Figure 7



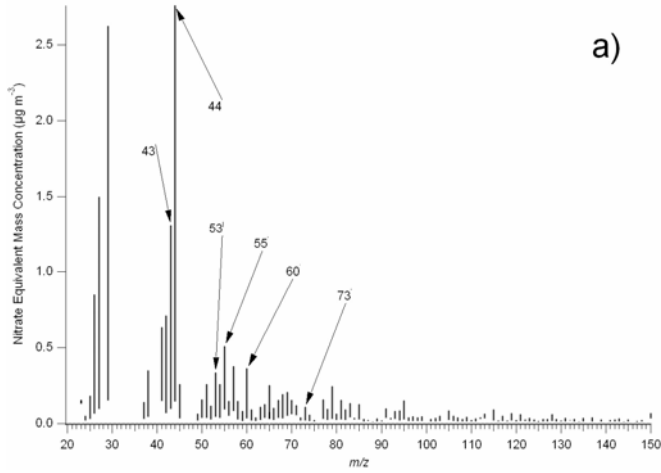
- 1
- 2
- 3

Figure 8

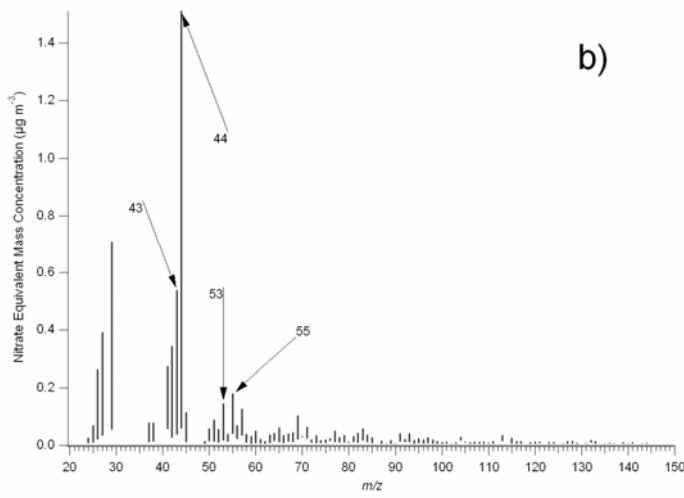


1  
2  
3  
4

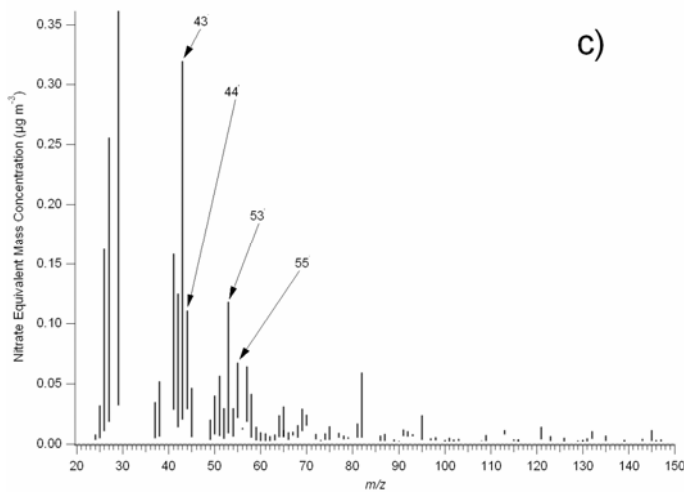
Figure 9



1



2



3

4

5

Figure 10